

# UC San Diego

## UC San Diego Previously Published Works

### Title

Model correction and updating of a stochastic degradation model for failure prognostics of miter gates

### Permalink

<https://escholarship.org/uc/item/5jm0r2vk>

### Authors

Jiang, Chen  
Vega, Manuel A  
Todd, Michael D  
[et al.](#)

### Publication Date

2022-02-01

### DOI

10.1016/j.ress.2021.108203

Peer reviewed

1 **A Novel Framework for Integration of Abstracted Inspection Data and Structural**  
2 **Health Monitoring for Damage Prognosis of Miter Gates**

3 Manuel A. Vega<sup>a</sup>, Zhen Hu<sup>b</sup>, Travis B. Fillmore<sup>c</sup>, Matthew D. Smith<sup>c</sup>, and Michael D. Todd<sup>a\*</sup>

4 <sup>a</sup> *Department of Structural Engineering,*  
5 *University of California San Diego,*  
6 *9500 Gilman Dr., La Jolla, California, USA 92093-0085*

7 <sup>b</sup> *Department of Industrial and Manufacturing Systems Engineering,*  
8 *University of Michigan-Dearborn,*  
9 *4901 Evergreen Rd., Dearborn, Michigan, USA 48187*

10 <sup>c</sup> *Coastal and Hydraulics Laboratory, Engineer Research and Development Center,*  
11 *US Army Corps of Engineers,*  
12 *3909 Halls Ferry Rd, Vicksburg, Mississippi, USA 39180*

13 **Abstract**

14 Operational condition assessments, using a discrete rating system, are frequently used by field  
15 engineers to assess inland navigation assets and components. Challenges such as the  
16 occasional inability to perform inspections (such as the case with locks watered in an  
17 operational state) and protocol requirements requiring ratings even when they aren't inspected  
18 lead to highly abstracted inspection data, which are also very prone to human error and  
19 misinterpretations due to inspections protocol. On the other hand, some navigational locks are  
20 equipped with structural health monitoring (SHM) systems to continuously perform  
21 assessments from data obtained *in situ*. This paper aims to develop a novel **hybrid** damage  
22 prognosis framework for miter gate component of navigational locks, by mitigating effects of  
23 human errors on the condition assessment and integrating the highly abstracted inspection data  
24 with the SHM. It overcomes two main challenges, namely (1) there is no physical or empirical  
25 model available to model the loss-of-contact degradation in the gate, and (2) the mismatches  
26 between the inspection data and the SHM system due to data abstraction. A practical case of  
27 monitoring loss-of-contact quoin block demonstrates the efficacy of the proposed framework.

28 **Keywords:** Miter Gates; Transition Matrix; Human Error; Gap Growth Model; Damage  
29 Estimation; Uncertainty

---

\* Corresponding author: University of California San Diego, 9500 Gilman Dr., La Jolla, California, USA 92093-0085, Email: mdtodd@eng.ucsd.edu

## Nomenclature

$a_t, a(t)$	=	gap length at time $t$
$a_e$	=	gap failure threshold
$a(i, j+k), a_{i, j+k}$	=	$i$ -th realization of the gap length at the $(j+k)$ -th time step
$\mathbf{a}_s(\boldsymbol{\theta}, \mathbf{e})$	=	Samples/realizations obtained of the gap length degradation model parametrized by $\boldsymbol{\theta}$ and $\mathbf{e}$
$\mathbf{e}$	=	vector of estimated parameters, $e_i$ , of mapping function, $h_s(a(t))$
$f_e(\mathbf{e} \boldsymbol{\theta})$	=	joint PDF of $e_i$ given $\boldsymbol{\theta}$
$g(t, \boldsymbol{\theta})$	=	degradation model of the miter gate damage gap at time $t$ given $\boldsymbol{\theta}$
$\hat{g}(a_{k+1}, \mathbf{x}_{k+1})$	=	FE model or surrogate model as a function of $a_{k+1}$ and $\mathbf{x}_{k+1}$
$g_{opt}(\boldsymbol{\theta}; \boldsymbol{\beta}, \mathbf{R})$	=	cost/error function to tune degradation model given $\boldsymbol{\theta}, \boldsymbol{\beta}$ , and $\mathbf{R}$
$h_{OCA}(a_t, \boldsymbol{\beta})$	=	protocol mapping function given $\boldsymbol{\beta}$ to map gap length at time $t$ to OCA ratings
$h_s(a(t))$	=	estimated mapping function to map gap length at time $t$ to OCA ratings
$I_{j,t+1}$	=	inspected state $I_j$ (e.g. $A, B, C, D, F$ or $CF$ ) at time $t+1$
$I_{t+1}^u$	=	underlying true OCA rating at time $t+1$
$I_{t+1}^{obs}$	=	reported OCA rating from field engineers at time $t+1$
$I_{j,t+1}^s$	=	inspected state $I_j$ (e.g. $A, B, C, D, F$ or $CF$ ) at time $t+1$ obtained from degradation model
$n_{MCS}$	=	number of samples of stochastic degradation model at each time step
$N_d$	=	distinct degradation stages
$N_{PF}$	=	number of samples used in the state estimation
$N_s$	=	number of strain sensors providing data

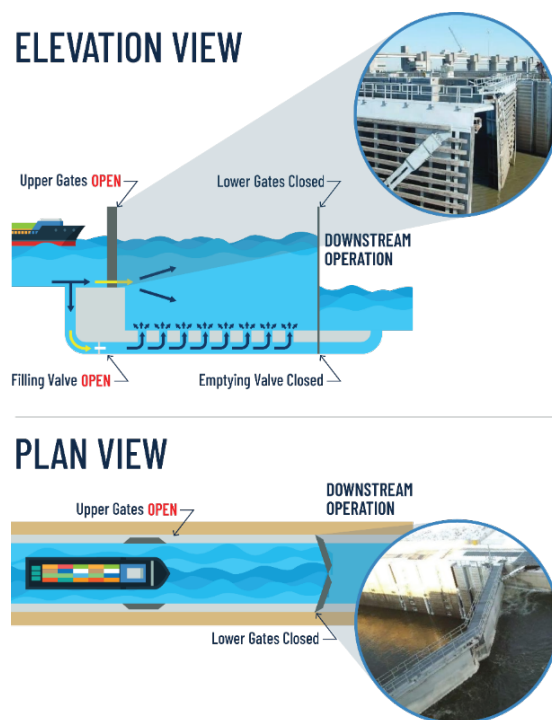
$N_t$	=	total number of simulation time steps for stochastic degradation model
$\mathbf{P}$	=	rating transition matrix
$\mathbf{P}_{\text{human}}$	=	human observation error matrix
$\mathbf{P}_{\text{OCA}}$	=	true OCA transition matrix
$\mathbf{P}_{\text{Report}}$	=	reported OCA transition matrix
$\hat{\mathbf{P}}(\boldsymbol{\theta})$	=	simulated transition probabilities of the OCA ratings from the degradation model simulation for given $\boldsymbol{\theta}$
$P_{ik}^h$	=	probability that the reported OCA rating is $k$ given that the true OCA rating is $i$
$P_{ij}^{\text{OCA}}$	=	probability of transitioning from true OCA rating $i$ at time $t$ to true OCA rating $j$ at $t+1$
$P_{kq}^R$	=	probability of transitioning from reported OCA rating $k$ at time $t$ to reported OCA rating $q$ at $t+1$
$\Pr\{\cdot\}$	=	probability operator
$q_v$	=	time-invariant parameter that controls the rate of cooling
$Q$	=	degradation model parameter to be estimated
$Q_i$	=	degradation model parameter at degradation stage $i$ to be estimated
$R$	=	OCA rating obtained from continuous monitoring
$\mathbf{s}_i$	=	set of strain measurement data at time step $t_i$
$\mathbf{s}_{1:k}$	=	set of strain measurement data collected up to $t_k$
$s_{iN_S}$	=	strain measurement data at time step $t_i$ at the $N_S$ location
$t_l, t_u$	=	lower and upper bounds of the time duration of interest (e.g. 1 year)
$t_m$	=	time when damage threshold is reached
$T_{q_v}(t)$	=	artificial temperature (a time-varying global parameter)
$T_{\text{RUL}}$	=	remaining useful life
$U(t)$	=	stationary standard Gaussian process

$w$	=	degradation model parameter to be estimated
$w_i$	=	degradation model parameter at degradation stage $i$ to be estimated
$\mathbf{x}_{k+1}$	=	other FE model inputs such water levels and temperature in miter gates
$X(t)$	=	stationary lognormal stochastic process
$\beta$	=	vector of parameters of protocol mapping function
$\Delta\theta(t)$	=	a trial jump distance of the variable $\theta(t)$
$\varepsilon$	=	measurement noise
$\zeta_x$	=	parameter that controls the correlation of $X(t)$ over time
$\theta$	=	vector of model parameters of degradation
$\theta_j, \theta(t)$	=	vector of model parameters of degradation stage $j$ (or at time $t$ )
$\Lambda(E)$	=	indicator function such $\Lambda(E) = 1$ if event $E$ is true and $\Lambda(E) = 0$ if event $E$ is false
$\mu_i$	=	mean of Gaussian random variable, $e_i$
$\sigma_e$	=	standard deviation of $e_i$ uncorrelated measurement noise, $\varepsilon$
$\sigma_i$	=	standard deviation variable of degradation stage $i$
$\sigma_{obs}$	=	standard deviation of
$\sigma_x$	=	standard deviation of $X(t)$
$\phi(\cdot)$	=	PDF of the standard normal distribution

## 31 1 Introduction

32 Miter gates are common hydraulic steel structures that facilitate passage of boats and  
33 watercraft through inland navigation systems as shown in Figure 1. In the United States, the  
34 U.S. Army Corps of Engineers (USACE) maintains and operates 236 locks at 191 sites [1]. A  
35 closure of a lock due to maintenance or repairs can cost up to \$3 million per day to the US  
36 economy [2]. This is underscored by the fact that more than half of these structural assets,  
37 including miter gates, have surpassed their 50-year economic design life [3]. To help prioritize

38 maintenance and repairs, operational condition assessment (OCA) ratings are performed by  
39 USACE inspectors via visual inspections [4]. However, the OCA ratings are highly abstracted  
40 and are assigned at a varying frequency, which varies from every year to occurring to a  
41 maximum of every 5 years [5]. Recently, several miter gates were equipped with SHM systems  
42 that collect strain measurement data in real time [6]. These continuous monitoring systems aim  
43 to provide insight regarding deteriorating gates. However, a framework that integrates visual  
44 inspections and SHM for damage diagnosis and prognosis has not been developed yet.



45  
46 **Figure 1:** Navigation along miter gates

47 This paper first gives an overview of the type of damage present in some components of  
48 miter gates and how these components are condition-rated based on the field OCA ratings.  
49 Section 3 briefly reviews current approaches for failure prognostics of miter gates through the  
50 integration of OCA transition matrix with continuous structural health monitoring and proposes  
51 a new approach for damage diagnosis and prognosis via a new degradation model derived by  
52 mapping the abstracted inspection data into a multistage discrete-time degradation model. The  
53 damage diagnosis and prognosis consider the human errors of field engineers in the inspection

54 data. The integration of the derived degradation model with physics-based finite element (FE)  
55 model updating will also be studied to perform online damage diagnostics and estimation of  
56 the miter gate's remaining useful life. Finally, Section 4 summarizes the important findings of  
57 this work and suggest further steps to be taken.

58 Even though this paper considers a specific application in miter gate damage assessment  
59 and prognosis, the developed framework is quite generic; it is easily adaptable to other  
60 structural monitoring applications that involve abstracted condition rating data (e.g., like the  
61 OCA) and online health monitoring system, such as other miter gate failure modes (e.g.,  
62 corrosion or pre-tension loss) or other structures including bridges [7–9], pavements [10,11],  
63 offshore structures [12], and others [13].

64 The contributions of this paper are summarized as: (1) it addresses bias in the OCA ratings  
65 in the state-transition matrix caused by human observation errors; (2) it maps the abstracted  
66 rating state-transition matrix to a failure evolution model; (3) it demonstrates a failure  
67 diagnostics and prognostics procedure using structural health monitoring systems based on the  
68 failure evolution model; and (4) it demonstrates the developed framework on the very practical  
69 case of monitoring loss-of-contact quoin block damage (resulting in “gaps” between the gate  
70 and support wall).

71 In summary, this paper proposes a novel hybrid approach for condition-based maintenance  
72 where abstracted OCA ratings subjected to human reporting errors are used to derive a  
73 degradation model. Simultaneously, a SHM system is used for damage diagnostics and  
74 prognostics based on the derived degradation model. The proposed approach overcomes the  
75 challenges that there is no viable degradation model available and there is substantial  
76 heterogeneity (i.e., physics-based simulation data, OCA rating data, errors in the OCA rating  
77 data, and strain measurement data) in the sources used to inform damage prognostics of miter  
78 gate components. Note that, the role of prognosis includes predictions of the future state that

79 inform reliability estimates of the system [14–16]. Predictive capabilities allow informed life  
80 cycle management, which target to optimize a certain system performance criterion [17] (e.g.  
81 cost, availability, reliability, etc.). Moreover, prognosis capabilities enable engineers to turn  
82 available data into information that enhance the current knowledge of the system and also  
83 provides a policy to maintain the system optimally.

84

## 85 **2 Problem Statement**

86 As mentioned above, there are significant economic implications caused by navigation lock  
87 closure, and how to prioritize repairs or other maintenance actions for miter gate components  
88 is paramount to minimizing the consequence costs. To understand the prioritization process,  
89 there is a need to estimate the extent of damage (i.e., damage diagnosis), and to predict the  
90 evolution of damage into the future (i.e., damage prognosis). Any prognosis action  
91 fundamentally requires a degradation model of some kind. Ideally, this model would be built  
92 from existing time series data or by data generated using a physics-based knowledge of the  
93 degradation/failure process. However, in many real-world applications such as with this miter  
94 gate case, the lack of existing time series data correlated to deteriorating components and the  
95 lack of understanding of the physics behind the damage mechanism evolution impose  
96 additional challenges to performing damage prognosis.

97 As mentioned, OCA ratings are a primary tool used to inform the structural condition state.  
98 An OCA rating is a categorical rating given by an inspector, who bases the evaluation on a  
99 rating system developed by the USACE Asset Management team, which involves engineering  
100 knowledge and information of pre-existing inspections. This rating system classifies structural  
101 and non-structural components as A (Excellent), B (Good), C (Fair), D (Poor), F (Failing) and  
102 CF (Completely Failed). More detailed definitions can be found in [3]. These ratings are given  
103 at the component level of the structural asset (e.g., the miter gate quoin blocks in this paper).



104 These discrete ratings are highly abstracted, assigned at varying time intervals, and are very  
105 prone to human error and to misinterpretations due to inspections protocol [16]. However, these  
106 ratings can provide information regarding transitions between different damage rating  
107 categories, which may be used to build a degradation model parametrized according to the  
108 deterioration of the OCA inspection ratings. In this application, the deterioration of a quoin  
109 block component in a miter gate (“damage”) is manifested as a “gap” that results in loss of  
110 contact beyond the “regular gap” tolerance ( $\sim 1/32$  in.) between the quoin block attached to the  
111 gate and the quoin block attached to the wall that supports the gate laterally. The “regular gap”  
112 tolerance allows a miter gate to operate and closes when the gate is subjected to hydrostatic  
113 loading. The formation of an undesirable “damage gap” beyond the tolerance controls the  
114 lateral boundary condition of a miter gate, and significant changes can lead to higher  
115 strain/stress in critical components (e.g., the pintle) of the gate. The “gap” or “damage gap” in  
116 the subsequent sections of this paper is thus the target damage mechanism considered in this  
117 work. More details regarding the different miter gates components mentioned (e.g. quoin  
118 blocks, pintle, etc.) can be found here [2].

119 From historical inspections, a database of the OCA ratings for quoin blocks and other  
120 components is available for the past several years, which provides information of the gap  
121 transition over the year at the abstracted OCA rating level. Even though the OCA ratings are  
122 very prone to human errors, they are the only available data source that contains some form of  
123 degradation information of the gate at present. The problem that needs to be solved is how to  
124 utilize the abstracted information to effectively perform failure prognostics. In this paper, these  
125 reported ratings would be used to build a transition matrix. This reported transition matrix  
126 would be combined with a human error matrix to improve the prognosis capabilities of the  
127 damage mechanism. This human error matrix will quantify the ability of the inspector to  
128 perform correct assessments and false positives/negatives assessments. Diagnosis and

129 prognosis using data-driven models built from solely inspection data (i.e. OCA ratings),  
130 however, may lead to large uncertainty in the failure prognosis as shown in previous studies  
131 [16,18] and in the case study section.

132 Beyond these condition ratings, however, structural health monitoring (SHM) systems have  
133 been developed for the miter gates to measure their distributed point strain response during  
134 operation, providing continuous data streams which may be mined for damage-related  
135 information. The SHM measurement systems are coupled with validated high-fidelity physics-  
136 based finite element (FE) models [16,19–22], allowing for inference/estimation of the damage  
137 gap using the strain measurements. This approach provides more confident estimates of the  
138 damage gap state over time. While it is true that the SHM system increases gap inference  
139 capabilities, it cannot be used directly to predict the gap degradation over time, since the  
140 physics of the gap degradation is complex and not fully understood; SHM alone is not enough  
141 to inform decisions regarding prioritizing preventive maintenance.

142 As described above, however, the historical OCA ratings nevertheless do contain  
143 information that may be used to understand the gap degradation over time, even though it is  
144 highly abstracted and may be contaminated by human observation errors or bias. Synthesizing,  
145 rather than separating, OCA rating transition information and SHM system information has the  
146 potential to improve an integrated state awareness (damage state) and state prediction (future  
147 damage state).

148 The two lines of enquiry that are addressed in this paper, therefore, may be summarized as  
149 follows:

- 150 (1) How should the highly abstracted OCA rating transition information be connected with  
151 a high-fidelity FE model for useful integrated damage diagnosis and prognosis?
- 152 (2) How should the effects of errors in the OCA rating transition information be mitigated  
153 for the damage diagnosis and prognosis?

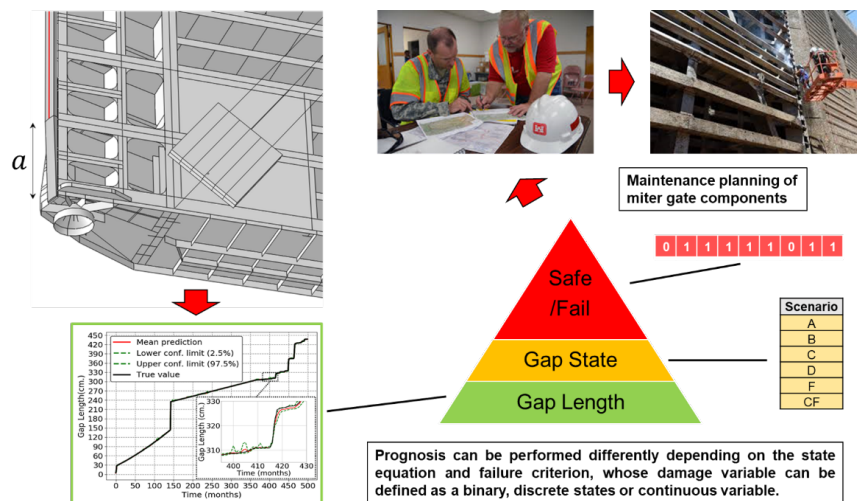
154

### 155 3 Proposed Method

156 In this section, a brief review of current methods for failure prognosis of miter gates is  
157 summarized. After that, the proposed method is explained in detail.

#### 158 3.1 Overview

159 Figure 2 shows the state (damage) variable hierarchy for bearing gaps in a quoin block.  
160 This figure shows a hierarchy pyramid that contain three different ways that the gap can be  
161 described. The most basic one would use a binary system that would define the state as  
162 damaged or undamaged, as time evolves. The next one would be based on discrete state-  
163 transition system such as the OCA ratings. For the two ways mentioned, the determination of  
164 these deterioration or damage labels would be based on an asset management protocol.



165

166 **Figure 2:** State (damage) variable hierarchy for bearing gap in quoin block

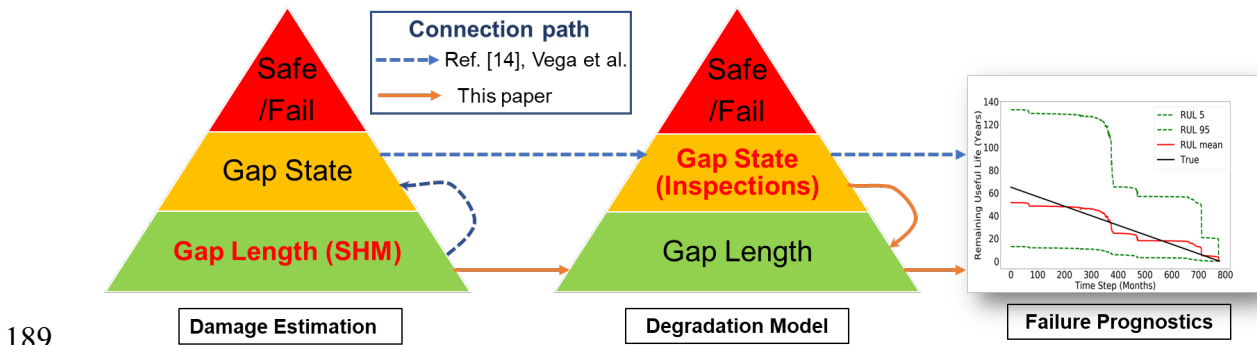
167 Based on a large historical OCA database, the number of times that a component  
168 transitioned from one rating category to another (as determined by engineering expert  
169 elicitation) over a given inspection time step can be determined to generate the rating transition  
170 matrix [23]. The transition matrix  $\mathbf{P}$  (see Eq. (1)) is defined as a square matrix with nonnegative  
171 values that represents how some process “transitions” from one state to the next. In this

172 application, an inspected state at time  $t$ ,  $I_{i,t}$ , (with  $i = 1 \dots 6$ , corresponding to the 6 letter ratings  
 173 specified above), will transition to inspected state at time  $t + 1$ ,  $I_{j,t+1}$ ,  $j = 1 \dots 6$ , according to

$$174 \quad \mathbf{P} = P(I_{j,t+1} | I_{i,t}) = \begin{bmatrix} P(I_{1,t+1} = A | I_{1,t} = A) & \cdots & P(I_{6,t+1} = CF | I_{1,t} = A) \\ \vdots & \ddots & \vdots \\ P(I_{1,t+1} = A | I_{6,t} = CF) & \cdots & P(I_{6,t+1} = CF | I_{6,t} = CF) \end{bmatrix}. \quad (1)$$

175 In Eq. (1), only the upper triangular components were considered to simulate component  
 176 deterioration; the lower triangular components would represent improvements or repairs  
 177 (transitions from a worse condition to a better condition), and for the purposes of this analysis,  
 178 they were ignored. Further details on this transition matrix can be found in [16,24,25].

179 Furthermore, the bearing gaps may also be modelled at the continuous level (i.e. gap-length  
 180 level at the bottom of the pyramid) based on continuous structural health monitoring (SHM)  
 181 systems. In order to address the above-mentioned *first line of enquiry*, which is to connect the  
 182 highly abstracted OCA rating transition information with a high-fidelity FE model for useful  
 183 integrated damage diagnosis and prognosis, Vega et al. [16] developed a hybrid prognostic  
 184 approach by converting the continuous level into gap-state level as illustrated in Fig. 3. Even  
 185 though the approach developed in [16] allows for the integration of SHM with Markov analysis  
 186 for integrated damage diagnosis and prognosis, the component degradation modeling at the  
 187 discrete state-transition level could lead to wide uncertainty in the prognostics even when using  
 188 recursive model updating.



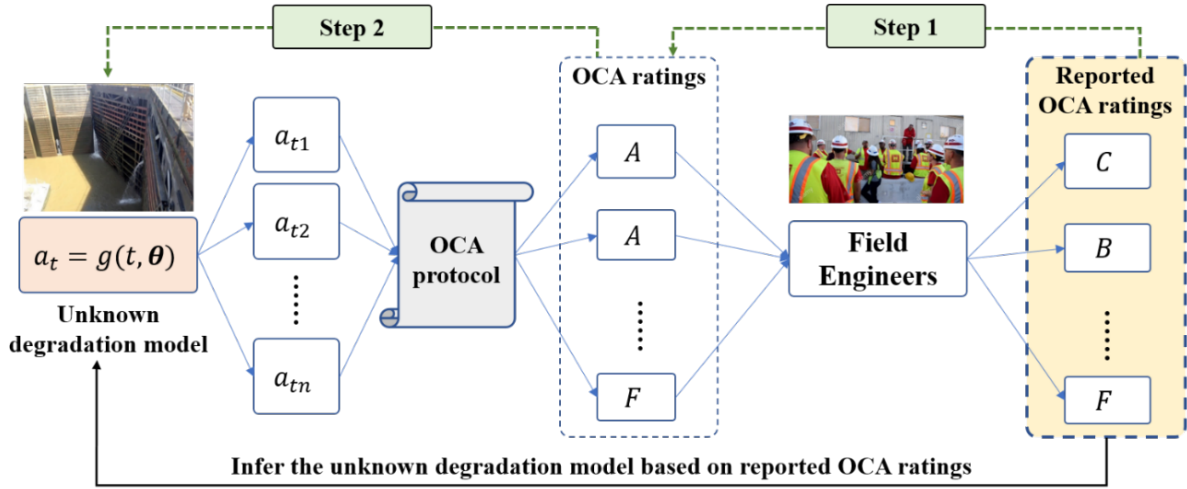
190 **Figure 3:** Comparison of the connection paths between damage estimation and degradation  
191 model for the methods presented in Vega et al. [16] and this paper

192 In this paper, as illustrated in Fig. 3, instead of converting the damage estimation at gap-  
193 length level into abstracted gap-state level for prognostics, the degradation model is built at the  
194 continuous gap-length level by tuning the degradation model parameters to agree with the  
195 Markov transition matrix built from the OCA ratings (gap-state level). After that, failure  
196 prognostics at the gap-length level is performed. The goal is to meaningfully increase the  
197 confidence in the miter gate failure prognostics beyond on what is was proposed in [16] to  
198 achieve an effective and useful decision-making capability. In addition to the tuning of  
199 degradation model parameters using data at gap-state level, a new approach will also be  
200 developed to address the errors in the OCA transition matrix due to human observation  
201 variability, thereby addressing the *second line of enquiry* mentioned above).

202 Let  $a_t = g(t, \boldsymbol{\theta})$  be the underlying degradation model of the miter gate damage gap, where  
203  $a_t$  is the gap length at time  $t$ , and  $\boldsymbol{\theta}$  is a vector of model parameters. Fig. 4 shows the  
204 relationship among the degradation model, OCA ratings, and the reported OCA ratings by the  
205 field engineers. As shown in Fig. 4, the OCA protocol maps the gap length,  $a_t$ , (i.e., the output  
206 of the unknown degradation model) into OCA ratings as if the protocol were strictly and  
207 accurately followed by the field engineers. Due to human observation error and variability,  
208 however, the OCA ratings reported by the field engineers as indicated in Fig. 4 may not be the  
209 same as the “true” rating that better represents the condition; this is proven true for inspectors  
210 in many application domains [26].

211 One of the objectives of the proposed method is to infer the unknown degradation model,  
212  $a_t = g(t, \boldsymbol{\theta})$ , using *the reported OCA ratings*, which include the human variability or errors in  
213 the rating reporting process. The inferred degradation model will then be used for *integrated*

214 damage diagnostics and prognostics of the miter gate. As shown in Fig. 4, the inference of the  
 215 unknown degradation model in the proposed framework is accomplished through two steps:



216  
 217 **Figure 4:** Relationship among the gap degradation, OCA ratings, and the reported OCA  
 218 ratings

- 219 • **Step 1:** Mapping of the reported OCA ratings to the underlying condition for a given  
 220 OCA protocol, by considering the human observation errors of field engineers in  
 221 reporting.
- 222 • **Step 2:** Estimation of the degradation model parameters ( $\theta$ ) based on the obtained true  
 223 OCA ratings (i.e. true OCA transition matrix).

224 In the next section, these two steps will be explained in detail.

### 225 3.2 Mapping of the reported OCA rating transition matrix to the true transition matrix

226 In order to map the reported OCA rating transition matrix to the underlying “true” OCA  
 227 transition matrix, the underlying true OCA rating is defined at time  $t$  as  $I_t^{tr}$  and that at  $t+1$  as  
 228  $I_{t+1}^{tr}$ , the reported OCA rating from field engineers at time  $t$  as  $I_t^{obs}$  and that at time  $t+1$  as  $I_{t+1}^{obs}$ .  
 229 Based on these definitions, the true OCA transition matrix  $\mathbf{P}_{OCA}$  (i.e. OCA “ideal” protocol is  
 230 strictly followed) is denoted as

231

$$\mathbf{P}_{\text{OCA}} = \begin{bmatrix} P_{11}^{OCA} & P_{12}^{OCA} & \dots & P_{16}^{OCA} \\ 0 & P_{22}^{OCA} & \dots & P_{26}^{OCA} \\ \vdots & \vdots & \ddots & \vdots \\ 0 & 0 & \dots & P_{66}^{OCA} \end{bmatrix}, \quad (2)$$

232 where  $P_{ij}^{OCA} = \Pr\{I_{t+1}^{tr} = j | I_t^{tr} = i\} \triangleq P(I_{j,t+1}^{tr} | I_{i,t}^{tr})$ ,  $\forall i = 1, 2, \dots, 6; j = i, \dots, 6$  represents the  
 233 probability of transitioning from **true** OCA rating  $i$  at time  $t$  to **true** OCA rating  $j$  at  $t+1$ .

234 Similarly, the reported transition matrix, built from the OCA ratings reported by field  
 235 engineers, is denoted as

236

$$\mathbf{P}_{\text{Report}} = \begin{bmatrix} P_{11}^R & P_{12}^R & \dots & P_{16}^R \\ 0 & P_{22}^R & \dots & P_{26}^R \\ \vdots & \vdots & \ddots & \vdots \\ 0 & 0 & \dots & P_{66}^R \end{bmatrix}, \quad (3)$$

237 where  $P_{kq}^R = \Pr\{I_{t+1}^{obs} = q | I_t^{obs} = k\}$ ,  $\forall k = 1, 2, \dots, 6; q = k, \dots, 6$  is the probability of transitioning  
 238 from **reported** OCA rating  $k$  at time  $t$  to **reported** OCA rating  $q$  at  $t+1$ , based on the reported  
 239 OCA ratings. In addition, from the reported OCA ratings the state probabilities  
 240  $\Pr\{I_t^{obs} = k\}$ ,  $k = 1, 2, \dots, 6$  and  $\Pr\{I_{t+1}^{obs} = q\}$ ,  $q = 1, 2, \dots, 6$  may also be obtained.

241 The goal of Step 1 of the proposed method (see Fig. 4) is to map  $\mathbf{P}_{\text{Report}}$  to  $\mathbf{P}_{\text{OCA}}$ . To achieve  
 242 this goal, the human observation error matrix is defined as

243

$$\mathbf{P}_{\text{human}} = \begin{bmatrix} P_{11}^h & P_{12}^h & \dots & P_{16}^h \\ 0 & P_{22}^h & \dots & P_{26}^h \\ \vdots & \vdots & \ddots & \vdots \\ 0 & 0 & \dots & P_{66}^h \end{bmatrix}, \quad (4)$$

244 in which  $P_{ik}^h = \Pr\{I_t^{obs} = k | I_t^{tr} = i\}$  is the probability that the reported OCA rating is  $k$  given  
 245 that the true OCA rating is  $i$ .

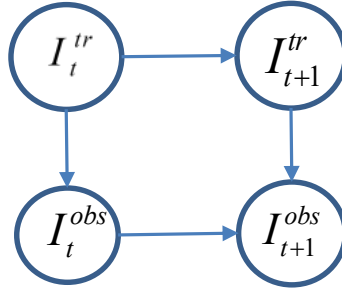
246 Based on the above definitions of  $\mathbf{P}_{\text{OCA}}$ ,  $\mathbf{P}_{\text{Report}}$ , and  $\mathbf{P}_{\text{human}}$ , the reported and true OCA  
 247 ratings are connected using a Bayesian network as shown in Fig. 5.

248 From the above Bayesian network, the following conditional probability tables (CPTs) are  
 249 obtained:

$$\begin{aligned}
 250 \quad & \Pr\{I_t^{obs} = k \mid I_t^{tr} = i\} = P_{ik}^h, \forall i = 1, 2, \dots, 6; k = 1, 2, \dots, 6; \\
 & \Pr\{I_{t+1}^{obs} = q \mid I_{t+1}^{tr} = j\} = P_{jq}^h, \forall j = 1, 2, \dots, 6; q = 1, 2, \dots, 6;
 \end{aligned} \tag{5}$$

251 and

$$\begin{aligned}
 & \Pr\{I_{t+1}^{obs} = q \mid (I_{t+1}^{tr} = j, I_t^{obs} = k)\} \\
 252 \quad & = \frac{\Pr\{I_{t+1}^{obs} = q, I_{t+1}^{tr} = j, I_t^{obs} = k\}}{\Pr\{I_{t+1}^{tr} = j, I_t^{obs} = k\}}, \\
 & = \frac{\Pr\{I_t^{obs} = k \mid I_{t+1}^{obs} = q, I_{t+1}^{tr} = j\} \Pr\{I_{t+1}^{obs} = q \mid I_{t+1}^{tr} = j\} \Pr\{I_{t+1}^{tr} = j\}}{\Pr\{I_{t+1}^{tr} = j, I_t^{obs} = k\}}.
 \end{aligned} \tag{6}$$



253 **Figure 5:** A Bayesian network connecting the observed and the true OCA ratings  
 254

255 Since the lower triangular components of  $\mathbf{P}_{\text{Report}}$  are all zero, the following marginal  
 256 probability is written

$$257 \quad \Pr\{I_{t+1}^{tr} = j, I_t^{obs} = k\} = \sum_{w=k}^6 \Pr\{I_{t+1}^{obs} = w, I_{t+1}^{tr} = j, I_t^{obs} = k\}. \tag{7}$$

258 With the above CPTs, the task is to obtain the true OCA transition matrix by solving  
 259  $\Pr\{I_{t+1}^{tr} = j \mid I_t^{tr} = i\}, \forall i = 1, 2, \dots, 6; j = 1, \dots, 6$  in the Bayesian network shown in Fig. 5. Using  
 260  $\Pr\{I_{t+1}^{obs} = q\}, q = 1, 2, \dots, 6$ , the following marginal probability is written



261 
$$\Pr\{I_{t+1}^{obs} = q\} = \sum_{j=1}^6 \Pr\{I_{t+1}^{obs} = q, I_{t+1}^{tr} = j\}, \forall q = 1, 2, \dots, 6;$$

262 
$$= \sum_{j=1}^6 \Pr\{I_{t+1}^{obs} = q | I_{t+1}^{tr} = j\} \Pr\{I_{t+1}^{tr} = j\}, \forall q = 1, 2, \dots, 6,$$

(8)

262 which may be elucidated more clearly in matrix form as

263 
$$\begin{bmatrix} \Pr\{I_{t+1}^{obs} = 1\} \\ \Pr\{I_{t+1}^{obs} = 2\} \\ \vdots \\ \Pr\{I_{t+1}^{obs} = 6\} \end{bmatrix} = \begin{bmatrix} P_{11}^h & P_{12}^h & \dots & P_{16}^h \\ P_{21}^h & P_{22}^h & \dots & P_{26}^h \\ \vdots & \vdots & \ddots & \vdots \\ P_{61}^h & P_{62}^h & \dots & P_{66}^h \end{bmatrix} \begin{bmatrix} \Pr\{I_{t+1}^{tr} = 1\} \\ \Pr\{I_{t+1}^{tr} = 2\} \\ \vdots \\ \Pr\{I_{t+1}^{tr} = 6\} \end{bmatrix}.$$

(9)

264 Based on Eq. (9),  $\Pr\{I_{t+1}^{tr} = j\}, \forall j = 1, 2, \dots, 6$  may be solved using  $\mathbf{P}_{\text{human}}$  and

265  $\Pr\{I_{t+1}^{obs} = q\}, q = 1, 2, \dots, 6$ . In this paper, a constrained least-squares method is used to solve

266 Eq. (9) to ensure that the obtained probability estimates are in the range of  $[0, 1]$ . In order to

267 estimate  $\Pr\{I_{t+1}^{tr} = j | I_t^{tr} = i\}, \forall i = 1, 2, \dots, 6; j = i, \dots, 6$ , a derivation of the term

268  $\Pr\{I_t^{obs} = k, I_{t+1}^{obs} = q\} = P_{kq}^R \Pr\{I_t^{obs} = k\}$  is performed (see **Appendix A** for derivations) as

269 follows:

270 
$$P_{kq}^R \Pr\{I_t^{obs} = k\} = \sum_{i=1}^6 \sum_{j=i}^6 \left( \frac{\Pr\{I_t^{obs} = k | I_{t+1}^{obs} = q, I_{t+1}^{tr} = j\} P_{jq}^h \Pr\{I_{t+1}^{tr} = j\}}{\sum_{w=k}^6 \Pr\{I_t^{obs} = k | I_{t+1}^{obs} = w, I_{t+1}^{tr} = j\} P_{jw}^h \Pr\{I_{t+1}^{tr} = j\}} P_{ik}^h \right) \Pr\{I_{t+1}^{tr} = j, I_t^{tr} = i\}.$$

(10)

271 In order to make  $\Pr\{I_{t+1}^{tr} = j | I_t^{tr} = i\}, \forall i = 1, 2, \dots, 6; j = i, \dots, 6$  solvable given the current

272 available information ( $\mathbf{P}_{\text{Report}}$  and  $\mathbf{P}_{\text{human}}$ ), a conditional independence is assumed, given by

273  $\Pr\{I_t^{obs} = k | I_{t+1}^{obs} = q, I_{t+1}^{tr} = j\} = \Pr\{I_t^{obs} = k | I_{t+1}^{obs} = q\}$ . This is a reasonable assumption for the

274 Bayesian network structure given in Fig. 5, since the resulting joint probability mass function

275  $\Pr\{I_{t+1}^{obs} = q, I_{t+1}^{tr} = j, I_t^{obs} = k\}$  satisfies the constraints of all the current given information in

276  $\mathbf{P}_{\text{Report}}$  and  $\mathbf{P}_{\text{human}}$ . Based on this assumption, the conditional probability and Bayes rule are

277 exploited

$$\begin{aligned}
 & \Pr\{I_{t+1}^{obs} = q, I_{t+1}^{tr} = j, I_t^{obs} = k\} \\
 278 & = \Pr\{I_t^{obs} = k \mid I_{t+1}^{obs} = q\} P_{jq}^h \Pr\{I_{t+1}^{tr} = j\} = \frac{P_{kq}^R \Pr\{I_t^{obs} = k\} P_{jq}^h \Pr\{I_{t+1}^{tr} = j\}}{\Pr\{I_{t+1}^{obs} = q\}}, \forall q \geq k. \quad (11)
 \end{aligned}$$

279 Substituting Eq. (11) into Eq. (10) as follows

$$\begin{aligned}
 & P_{kq}^R \Pr\{I_t^{obs} = k\} \\
 280 & = \sum_{i=1}^6 \sum_{j=i}^6 \left( \frac{P_{kq}^R \Pr\{I_t^{obs} = k\} P_{jq}^h \Pr\{I_{t+1}^{tr} = j\}}{\Pr\{I_{t+1}^{obs} = q\}} \right) P_{ik}^h \Pr\{I_{t+1}^{tr} = j, I_t^{tr} = i\}. \quad (12)
 \end{aligned}$$

$$\begin{aligned}
 & \frac{P_{kq}^R \Pr\{I_t^{obs} = k\} P_{jq}^h \Pr\{I_{t+1}^{tr} = j\}}{\Pr\{I_{t+1}^{obs} = q\}} \\
 281 & \text{Defining } P_{ijkq} \triangleq \frac{P_{kq}^R \Pr\{I_t^{obs} = k\} P_{jq}^h \Pr\{I_{t+1}^{tr} = j\}}{\sum_{w=k}^6 \left( \frac{P_{kw}^R \Pr\{I_t^{obs} = k\} P_{jw}^h \Pr\{I_{t+1}^{tr} = j\}}{\Pr\{I_{t+1}^{obs} = w\}} \right)} P_{ik}^h, \text{ it follows that}
 \end{aligned}$$

$$282 \quad P_{kq}^R \Pr\{I_t^{obs} = k\} = \sum_{i,j=1}^6 P_{ijkq} \Pr\{I_{t+1}^{tr} = j, I_t^{tr} = i\} \quad (13)$$

283 which again elucidated in matrix form is

$$\begin{aligned}
 & \begin{bmatrix} P_{J,1} \\ P_{J,2} \\ \vdots \\ P_{J,20} \\ P_{J,21} \end{bmatrix}_{21 \times 1} = \begin{bmatrix} P_{J,1,1}^h & P_{J,1,2}^h & \cdots & P_{J,1,20}^h & P_{J,1,21}^h \\ P_{J,2,1}^h & P_{J,2,2}^h & \cdots & P_{J,2,20}^h & P_{J,2,21}^h \\ \vdots & \vdots & \ddots & \vdots & \vdots \\ P_{J,20,1}^h & P_{J,20,2}^h & \cdots & P_{J,20,20}^h & P_{J,20,21}^h \\ P_{J,21,1}^h & P_{J,21,2}^h & \cdots & P_{J,21,20}^h & P_{J,21,21}^h \end{bmatrix}_{21 \times 21} \begin{bmatrix} P_{J,1}^{OCA} \\ P_{J,2}^{OCA} \\ \vdots \\ P_{J,20}^{OCA} \\ P_{J,21}^{OCA} \end{bmatrix}_{21 \times 1}, \quad (14)
 \end{aligned}$$

285 where  $P_{J,x} = P_{kq}^R \Pr\{I_t^{obs} = k\}$ ,  $P_{J,y}^{OCA} = \Pr\{I_{t+1}^{tr} = j, I_t^{tr} = i\}$ ,  $P_{J,x,y}^h = P_{ijkq}^h$ , and the indices are

286 related to each other by

$$x = \begin{cases} q, & \text{if } k = 1 \\ (q - k + 1) + \sum_{s=1}^{k-1} (6 - s + 1), & \text{otherwise} \end{cases}, \forall q \geq k, \quad (15)$$

288 and

$$y = \begin{cases} j, & \text{if } i = 1 \\ (j - i + 1) + \sum_{s=1}^{i-1} (6 - s + 1), & \text{otherwise} \end{cases}, \forall j \geq i. \quad (16)$$

290 Using Eq. (14),  $P_{j,y}^{OCA} = \Pr\{I_{t+1}^{tr} = j, I_t^{tr} = i\}, \forall i = 1, 2, \dots, 6; j = i, \dots, 6$  may be solved  
 291 similarly as in Eq. (9) using the constrained least-squares method. Using the above equations  
 292 (Eq. (5) through (16)), the reported OCA rating transition matrix  $\mathbf{P}_{\text{Report}}$  is mapped into the  
 293 underlying true OCA rating transition matrix  $\mathbf{P}_{\text{OCA}}$  considering the human observation errors  
 294  $\mathbf{P}_{\text{human}}$ .

295 As shown above, the estimation of the  $\mathbf{P}_{\text{OCA}}$  matrix depends on the  $\mathbf{P}_{\text{human}}$  matrix, which is  
 296 assumed to be known in this work. However, when it is unknown, there are two approaches to  
 297 estimate the  $\mathbf{P}_{\text{human}}$  matrix. One way is to do a benchmark study using a statistically significant  
 298 set of data focused on visual OCA ratings, similar to [26]. This consists on bringing inspectors  
 299 to assess miter gate component with previously known damage condition to estimate  
 300  $P_{ik}^h = \Pr\{I_t^{obs} = k | I_t^{tr} = i\}$ . The other approach is to make the best possible estimation of  $\mathbf{P}_{\text{human}}$   
 301 , using previously collected data to inform a prior distribution for the parameters of the  
 302 degradation model (described in the next section, which can be later updated using the  
 303 continuous SHM data). This second approach, when used in conjunction with Bayesian  
 304 methods, is more desirable since it enables the continuous updating of the degradation model  
 305 for a specific case/structure using SHM data. Further work that is beyond the scope of this  
 306 paper would be required to fully address any of these mentioned approaches. The next section

307 will discuss how to estimate the degradation model parameters  $\theta$  of  $a_t = g(t, \theta)$  using the  
 308 transition matrix  $\mathbf{P}_{\text{OCA}}$ .

### 309 3.3 Estimation of the degradation model parameters

310 As noted in Step 2 in Fig. 4, in order to establish a connection between the degradation  
 311 model  $a_t = g(t, \theta)$  and the OCA transition matrix  $\mathbf{P}_{\text{OCA}}$ , a mapping function is defined for the  
 312 OCA protocol as below

$$313 \quad R = h_{\text{OCA}}(a_t, \beta) = \begin{cases} I_{1,t} = A, a \in [0, \beta_1] \\ I_{2,t} = B, a_t \in [\beta_1, \beta_2] \\ I_{3,t} = C, a_t \in [\beta_2, \beta_3] \\ I_{4,t} = D, a_t \in [\beta_3, \beta_4] \\ I_{5,t} = F, a_t \in [\beta_4, \beta_5] \\ I_{6,t} = CF, a_t \in [\beta_5, \infty) \end{cases}, \quad (17)$$

314 where  $R$  is the OCA rating,  $a_t$  is the gap length, and  $\beta = [\beta_1, \beta_2, \beta_3, \beta_4, \beta_5]$  is a vector of  
 315 parameters of the mapping function related to the OCA protocol.

316 In the proposed method, the unknown parameters  $\theta$  are estimated for given set of  
 317 parameters  $\beta$  that define the mapping function (i.e. Eq. (17)), given the degradation model  
 318  $a_t = g(t, \theta)$  and the true OCA transition matrix,  $\mathbf{P}_{\text{OCA}}$ , shown in Sec. 3.2. After that, diagnostics  
 319 and prognostics are performed based on the estimated  $\theta$ .

320 The task of estimating  $\theta$  relies on solving the following optimization problem

$$321 \quad \begin{aligned} \theta^* &= \arg \min_{\theta} \{g_{\text{opt}}(\theta; \beta, \mathbf{P}_{\text{OCA}})\}, \\ &s.t. \theta \in \Omega, \end{aligned} \quad (18)$$

322 where  $g_{\text{opt}}(\theta; \beta, \mathbf{P}_{\text{OCA}})$  is a cost function of the optimization model, and  $\Omega$  is the domain of  
 323  $\theta$ . In the above optimization model, the cost function  $g_{\text{opt}}(\theta; \beta, \mathbf{P}_{\text{OCA}})$  is defined as

$$\begin{aligned}
324 \quad \mathcal{G}_{opt}(\boldsymbol{\theta}; \boldsymbol{\beta}, \mathbf{P}_{OCA}) &= \left\| \hat{\mathbf{P}}(\boldsymbol{\theta}) - \mathbf{P}_{OCA} \right\|_2, \\
&= \sum_{i=1}^6 \sum_{j=i}^6 (\hat{P}(I_{j,t+1}^s | I_{i,t}^s; \boldsymbol{\theta}) - P(I_{j,t+1}^r | I_{i,t}^r))^2,
\end{aligned} \tag{19}$$

325 in which  $I_{i,t}^s$  and  $I_{j,t+1}^s$  are the inspected state (e.g.  $A, B, C, D, F$  or  $CF$ ) at time  $t$  and  $t+1$   
326 respectively obtained from the degradation simulation and mapping function,  $h_{OCA}(a_t, \boldsymbol{\beta})$ . For  
327  $P(I_{j,t+1}^r | I_{i,t}^r) \triangleq \Pr\{I_{t+1}^r = j | I_t^r = i\}$ , the reader can refer to the definitions of Eq. (2),  
328  $\hat{\mathbf{P}}(\boldsymbol{\theta}) \triangleq \{\hat{P}(I_{j,t+1}^s | I_{i,t}^s; \boldsymbol{\theta}), i = 1, 2, \dots, 6; j = i, \dots, 6\}$  is the simulated transition probabilities of the  
329 OCA ratings from the degradation model simulation for given  $\boldsymbol{\theta}$ , and  $\mathbf{P}_{OCA}$  is the true OCA  
330 transition matrix (i.e. Eq. (2)) obtained from Sec. 3.2 based on the reported OCA transition  
331 matrix and human observation error matrix.

332 It should be noted that, theoretically speaking, the optimization model Eq. (19) may also  
333 be formulated directly from the reported OCA transition matrix  $\mathbf{P}_{Report}$  perspective by coupling  
334 the approach developed in this section with the forward uncertainty propagation of the OCA  
335 ratings based on the human error observation matrices. That kind of formulation may be  
336 considered as an alternative approach to the proposed method and will be compared in future  
337 work. The benefit of using  $\mathbf{P}_{OCA}$  in Eq. (19) is two-fold: first, the identification of  $\mathbf{P}_{OCA}$  in Sec.  
338 3.2 allows to perform failure prognostics with  $\mathbf{P}_{OCA}$  instead of  $\mathbf{P}_{Report}$  using the approach  
339 developed in [16]. Using  $\mathbf{P}_{OCA}$  to replace  $\mathbf{P}_{Report}$  in transition matrix-based prognostics will  
340 improve the accuracy of failure prognostics since  $\mathbf{P}_{OCA}$  mitigates the effects of human  
341 observation errors. Second, the formulation given in Eq. (19) eliminates process of uncertainty  
342 propagation step from  $\mathbf{P}_{OCA}$  to  $\mathbf{P}_{Report}$  in estimating  $\boldsymbol{\theta}$ , which reduces the complexity of the  
343 optimization process.

344 As shown in Eq. (19), the estimation of  $\hat{\mathbf{P}}(\boldsymbol{\theta})$  for a given  $\boldsymbol{\theta}$  is the key for the optimization-  
 345 based method to minimize the L2 error norm between the underlying true OCA transition  
 346 matrix,  $\mathbf{P}_{\text{OCA}}$ , and the estimated transition matrix  $\hat{\mathbf{P}}(\boldsymbol{\theta})$  obtained from the estimated multi-stage  
 347 continuous degradation model. The next section will discuss in detail on how to estimate  $\hat{\mathbf{P}}(\boldsymbol{\theta})$   
 348 for a given  $\boldsymbol{\theta}$ . After that, an explanation will be given of how to solve Eq. (19) based on the  
 349 estimation of multi-stage continuous degradation model.

### 350 3.3.1 Prediction of OCA rating transition matrix $\hat{\mathbf{P}}(\boldsymbol{\theta})$ for given $\boldsymbol{\theta}$

#### 351 (a) Selection of degradation model

352 As mentioned earlier, there is a need for a degradation model whose OCA transition matrix  
 353 prediction,  $\hat{\mathbf{P}}(\boldsymbol{\theta})$ , resembles the true OCA transition matrix,  $\mathbf{P}_{\text{OCA}}$ . A variation of the stochastic  
 354 model proposed by Yang and Manning [27], which is referred as the Yang and Manning model  
 355 and reviewed in Appendix B, is used. This model allows flexibility when considering the  
 356 abstracted OCA data and the lack of the understanding of the physics of the damage evolution  
 357 of bearing gaps.

358 To account for the effect of degradation stages over continuous time, the Yang and  
 359 Manning model (see Appendix B for details) is generalized as below

$$360 \quad \frac{da(t)}{dt} = \exp(\sigma(t)U(t))Q(t)(a(t))^{w(t)}, \quad (20)$$

361 where  $U(t)$  is a stationary standard Gaussian process with auto-correlation function given by  
 362 Eq. (51) in Appendix B,  $\sigma(t)$ ,  $Q(t)$ , and  $w(t)$  are parameters determined through gap length  
 363  $a(t)$  as follows

$$364 \quad \begin{cases} \sigma(t) = \sigma_j \\ Q(t) = Q_j, \text{ where } j = h_s(a(t)), \forall j = 1, \dots, N_d, \\ w(t) = w_j \end{cases} \quad (21)$$

365 in which  $N_d$  is the number of degradation stages,  $j = h_s(a(t))$  is a function that discretely  
 366 maps gap length  $a(t)$  into degradation stages as below

$$367 \quad j = h_s(a(t)) = \begin{cases} 1, & \text{if } a(t) \in [0, e_1], \\ 2, & \text{if } a(t) \in [e_1, e_2], \\ \vdots & \\ N_d, & \text{if } a(t) \in [e_{N_d-1}, \infty), \end{cases} \quad (22)$$

368 where  $e_i < e_{i+1}$ ,  $\forall i = 1, 2, \dots, N_d - 2$  are the threshold gap lengths that determine the transition  
 369 of degradation stages. Note that the mapping function  $j = h_s(a(t))$  for the gap growth model  
 370 is different from the mapping function (i.e.  $R = h_{OCA}(a_t, \boldsymbol{\beta})$ ) defined by the OCA protocol. The  
 371 mapping function  $j = h_s(a(t))$  is governed by the underlying degradation physics, while  
 372  $R = h_{OCA}(a_t, \boldsymbol{\beta})$  is defined by the engineers using OCA protocols.

373 Moreover, in order to account for the randomness of the threshold gap lengths that govern  
 374 the transition of degradation stages,  $e_i$ ,  $\forall i = 1, 2, \dots, N_d - 1$  are described as Gaussian random  
 375 variables as follows

$$376 \quad e_i \sim N(\mu_i, \sigma_e^2), \forall i = 1, 2, \dots, N_d - 1, \quad (23)$$

377 with mean  $\mu_i$  and standard deviation  $\sigma_e$ .

378 In the discrete time domain, the above degradation model is rewritten as

$$379 \quad a(t_{k+1}) = a(t_k) + \exp(\sigma(t_{k+1})U(t_{k+1}))Q(t_{k+1})(a(t_k))^{w(t_{k+1})}, \forall k = 1, 2, \dots, N_t, \quad (24)$$

$$380 \quad \begin{cases} \sigma(t_{k+1}) = \sigma_j \\ Q(t_{k+1}) = Q_j, \text{ where } j = h_s(a(t_k)), \forall j = 1, \dots, N_d, \\ w(t_{k+1}) = w_j \end{cases} \quad (25)$$

381 where  $N_t$  is the number of analysis time steps in the time duration of interest.

382 To summarize, in the selected degradation model, the parameters  $\boldsymbol{\theta}$  of the degradation  
 383 model include the following parameters

$$384 \quad \boldsymbol{\theta} \triangleq \{\boldsymbol{\theta}_1, \boldsymbol{\theta}_2, \dots, \boldsymbol{\theta}_{N_d}, \zeta, \mu_1, \mu_2, \dots, \mu_{N_d-1}, \boldsymbol{\sigma}_e\}, \quad (26)$$

385 where  $\boldsymbol{\theta}_j \triangleq \{\sigma_j, Q_j, w_j, j = 1, 2, \dots, N_d\}$ .

386 The next section will discuss the prediction of  $\hat{\mathbf{P}}(\boldsymbol{\theta})$  for a given  $\boldsymbol{\theta}$ .

387 (b) Prediction of  $\hat{\mathbf{P}}(\boldsymbol{\theta})$  using the degradation model

388 Based on the above degradation model, for given  $\boldsymbol{\theta}$  and  $\mathbf{e}$ , according to the derivations  
 389 given in **Appendix C**,  $\hat{P}(I_{j,t+1}^s | I_{i,t}^s; \boldsymbol{\theta}, \mathbf{e})$ ,  $\forall i = 1, 2, \dots, 6; j = i, \dots, 6$ , are estimated based on  
 390 the degradation simulation as follows

$$391 \quad \begin{aligned} & \hat{P}(I_{j,t+1}^s | I_{i,t}^s; \boldsymbol{\theta}, \mathbf{e}) \\ & \approx \frac{1}{(N_t - 12)n_{MCS}} \sum_{k=1}^{N_t-12} \frac{\sum_{q=1}^{n_{MCS}} \Lambda((\beta_{i-1} \leq a_{q,k} < \beta_i) \cap (\beta_{j-1} \leq a_{q,k+12} < \beta_j))}{\sum_{q=1}^{n_{MCS}} \Lambda(\beta_{i-1} \leq a_{q,k} < \beta_i)}, \end{aligned} \quad (27)$$

392 where  $\Lambda(\cdot)$  is an indicator function defined in Eq. (58) in Appendix C and  $a_{q,k}$  is the simulated  
 393  $q$ -th realization of gap length at time step  $t_k$  (see Appendix C for details).

394 The above probability estimate is conditioned on  $\boldsymbol{\theta}$  and  $\mathbf{e}$ . After considering the  
 395 uncertainty in threshold gap lengths,  $\mathbf{e} = [e_1, e_2, \dots, e_{N_d-1}]$  that determine the transition of  
 396 degradation stages, the marginalization of  $\hat{P}(I_{j,t+1}^s | I_{i,t}^s; \boldsymbol{\theta})$  may be written as

$$397 \quad \begin{aligned} \hat{P}(I_{j,t+1}^s | I_{i,t}^s; \boldsymbol{\theta}) &= \int \hat{P}(I_{j,t+1}^s | I_{i,t}^s; \boldsymbol{\theta}, \mathbf{e}) f_e(\mathbf{e} | \boldsymbol{\theta}) d\mathbf{e}, \\ &= \int \int \dots \int \hat{P}(I_{j,t+1}^s | I_{i,t}^s; \boldsymbol{\theta}, \mathbf{e}) \prod_{k=1}^{N_d-1} \phi\left(\frac{e_k - \mu_k}{\sigma_k}\right) de_1 de_2 \dots de_{N_d-1}, \end{aligned} \quad (28)$$



398 where  $f_e(\mathbf{e} | \boldsymbol{\theta})$  is the joint PDF of  $e_i$ , and  $e_i < e_{i+1}, \forall i = 1, 2, \dots, N_d - 2$ , and  $\phi(\cdot)$  is the PDF of  
 399 the standard normal distribution.

400 In this paper, a sampling-based approach is employed to estimate Eq. (28). **Using the above**  
 401 **equations and derivations in Appendix C**,  $\hat{\mathbf{P}}(\boldsymbol{\theta}) \triangleq \{\hat{P}(I_{j,t+1}^s | I_{i,t}^s; \boldsymbol{\theta}), i = 1, 2, \dots, 6; j = i, \dots, 6\}$   
 402 may be estimated for given  $\boldsymbol{\theta}$ . The estimated  $\hat{\mathbf{P}}(\boldsymbol{\theta})$  may then be used in Eq. (19) to obtain the  
 403 parameters  $\boldsymbol{\theta}$  of the degradation model. Table 1 provides a pseudocode for this process.

404 **Table 1:** Estimation of  $\hat{\mathbf{P}}(\boldsymbol{\theta})$  for given  $\boldsymbol{\theta} \triangleq \{\boldsymbol{\theta}_1, \boldsymbol{\theta}_2, \dots, \boldsymbol{\theta}_{N_d}, \zeta, \mu_1, \mu_2, \dots, \mu_{N_d-1}, \sigma_e\}$

Step	Description
1	<b>Initialization:</b> Generate samples of $U(t_1), \dots, U(t_{N_t})$ for a given correlation length $\zeta$ , samples of $e_i < e_{i+1}, \forall i = 1, 2, \dots, N_d - 2$ based on $\mu_1, \mu_2, \dots, \mu_{N_d-1}, \sigma_e$ , and initial samples of $a(t_0)$
2	Sort the samples of $e_i < e_{i+1}, \forall i = 1, 2, \dots, N_d - 1$
3	<b>For</b> $k = 1, 2, \dots, N_t$ :
4	Map gap length $a(t_{k-1})$ into degradation stage using Eq. (22)
5	Obtain samples of $a(t_k)$ using Eqs. (24) and (25)
<b>End</b>	
6	Obtain samples of $a(t_k), k = 1, 2, \dots, N_t$
7	Reshape the data and obtain samples of $a(t_k)$ and $a(t_k + 12)$
8	Compute $\hat{\mathbf{P}}(\boldsymbol{\theta})$ using Eqs. (27) and (28) for a given $\boldsymbol{\beta}$ defined in Eq. (17)

405 The next section discusses how to estimate  $\boldsymbol{\theta}$  by solving the optimization model given in  
 406 Eq. (19).

### 407 3.3.2 Estimation of degradation model parameters $\boldsymbol{\theta}$

408 In this paper, the Generalized Simulated Annealing (GSA) method is used to solve the  
 409 optimization problem. This method is a stochastic approach for approximating the global  
 410 optimum of the cost function shown in Eq. (19). The GSA method is mainly used when  
 411 processing complicated non-linear objective functions with a large number of local minima.

412 The Cauchy-Lorentz visiting distribution is used to generate a trial jump distance  $\Delta\theta(t)$  of the  
 413 variable  $\theta(t)$ ,

$$414 \quad \Delta\theta(t) \propto \frac{[T_{q_v}(t)]^{\frac{D}{3-q_v}}}{[1+(q_v-1)\frac{p^2}{2}]^{\frac{1}{q_v-1}+\frac{D-1}{2}}}, p \sim U(0,1), T_{q_v}(t) = T_{q_v}(1) \frac{2^{q_v-1}-1}{(1+t)^{q_v-1}-1}, \quad (29)$$

$$[T_{q_v}(t)]^{\frac{D}{3-q_v}}$$

415 where  $D$  is the dimension of the variable space,  $T_{q_v}(t)$  is the artificial temperature (a time-  
 416 varying global parameter), and  $q_v$  is a time-invariant parameter that controls the rate of  
 417 cooling. To avoid local minima, the trial jump uses an acceptance probability using a  
 418 Metropolis algorithm. In other words, the proposed trial jump is always accepted if it is  
 419 downhill and it is accepted with a probability if the jump is uphill, which allows to explore the  
 420 space outside the local minima. For more details on this method, the reader is referred to  
 421 [28,29].

422 After the parameters  $\theta$  are estimated, the degradation model can be used for damage  
 423 diagnostics and prognostics, which is briefly discussed in the next section.

### 424 3.4 Diagnostics and prognostics of using the degradation model

425 Let  $\mathbf{s}_i = [s_{i1}, s_{i2}, \dots, s_{iN_s}]$  be the strain measurement data at time step  $t_i$ , where  $N_s$  is the  
 426 number of strain sensors providing data. The degradation model  $a_t = g(t, \theta)$  obtained in Sec.  
 427 3.3 can then be used for failure diagnostics and prognostics using the approach presented in  
 428 Vega et al. [16], using the following state and measurement equations,

$$429 \quad \begin{aligned} \text{State equation: } a_{k+1} &= a_k + \exp(\sigma_{k+1} U_{k+1}) Q_{k+1} (a_k)^{w_{k+1}}, \\ \text{Measurement equation: } \mathbf{s}_{k+1} &= \hat{g}(a_{k+1}, \mathbf{x}_{k+1}) + \varepsilon, \end{aligned} \quad (30)$$

430 where  $a_{k+1}$ ,  $a_k$ ,  $\sigma_{k+1}$ ,  $U_{k+1}$ ,  $Q_{k+1}$ , and  $w_{k+1}$  are, respectively,  $a(t_{k+1})$ ,  $a(t_k)$ ,  $\sigma(t_{k+1})$ ,  $U(t_{k+1})$ ,  
 431  $Q(t_{k+1})$ , and  $w(t_{k+1})$  given in Eq. (24). The term  $\hat{g}(a_{k+1}, \mathbf{x}_{k+1})$  is a model (e.g., the FE model)  
 432 for the prediction of strain response for given gap state  $a_{k+1}$  and other input variables  $\mathbf{x}_{k+1}$  such  
 433 as water levels and temperature. The measurement noise  $\varepsilon$  is assumed to be normal,  
 434  $\varepsilon \sim N(\mathbf{0}, \sigma_{obs}^2 \mathbf{I})$ , with uncorrelated structure characterized by the standard deviation  $\sigma_{obs}$ .

435 Since the original FE model  $\hat{g}(a_{k+1}, \mathbf{x}_{k+1})$  is usually expensive, a trained and verified  
 436 surrogate model,  $\hat{g}(a_{k+1}, \mathbf{x}_{k+1})$ , is usually used to replace the original FE model. In this paper,  
 437 a Kriging surrogate modelling method is employed as it can effectively quantify the uncertainty  
 438 in the prediction, which is advantageous over pointwise-estimate surrogate modelling methods,  
 439 such as Neural Networks, Support Vector Machine, etc.

440 The equations above can then be solved recursively in a timely manner as been discussed  
 441 in Vega et al. [16]. Based on the failure diagnostics and prognostics of the gap growth, the  
 442 remaining useful life of a miter gate can be estimated at every time step  $t_k$  as

$$443 \quad \Pr\{T_{RUL} \leq t_m | \mathbf{s}_{1:k}\} = \frac{1}{N_{PF}} \sum_{i=1}^{N_{PF}} \Lambda\{a(i, j+k) > a_e, \exists j = 1, 2, \dots, m\}, \quad (31)$$

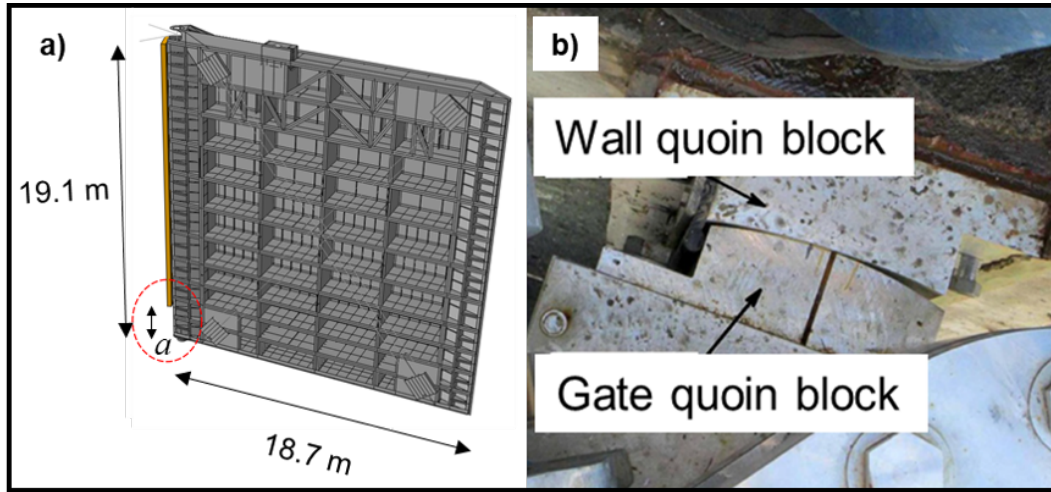
444 in which  $T_{RUL}$  stands for the remaining useful life,  $N_{PF}$  is the number of samples used in the  
 445 state estimation using Eq. (30),  $a_e$  is the gap failure threshold, and  $a(i, j+k)$  is the  $i$ -th  
 446 realization of the gap length at the  $(j+k)$ -th time step. In the next section, a miter gate case  
 447 study is used to demonstrate the effectiveness of the proposed framework.

448

#### 449 **4 A Case Study**

450 One of the primary concerns of USACE engineers for inspection, maintenance, and repair  
 451 are the condition of the quoin blocks [3]. Commonly, the deterioration of the quoin blocks is

452 broadly manifested as a small bearing “gap”. The formation of this gap is due to the contact  
 453 degradation between the quoin block attached to the gate and the quoin block attached to the  
 454 wall that supports the gate laterally. The formation of the bearing gap can be detected using  
 455 sensor data or from features derived from this data [2,19,30–32]. Figure 6 idealizes the loss of  
 456 contact in the physical-based FE model and shows the top view of the quoin blocks.



457  
 458 **Figure 6:** a) Gap formation at the bottom of the quoin blocks and b) the top view of the  
 459 contact between the quoin blocks [33]

460 The term  $\hat{P}(I_{j,t+1} | I_{i,t}, \theta)$  is the derived transition matrix obtained from the stochastic  
 461 degradation model. To calculate this matrix, it is necessary to map the gap length value from  
 462 its continuous form to the discrete OCA ratings using  $\beta$  defined in Eq. (17).  $\beta$  is also needed  
 463 in the evaluation of gap length using OCA ratings by the field engineers. Table 2 shows the  
 464 mapping between gap length,  $a(t)$ , to its corresponding OCA rating. For the values on this  
 465 table, the mapping is assumed to be known and would be treated as the inspection policy.

466 **Table 2:** Mapping from gap length,  $a(t)$ , to discrete OCA ratings.

Gap length (cm)	OCA rating
$0 \leq a < 76.2$	A
$76.2 \leq a < 152.4$	B
$152.4 \leq a < 228.6$	C
$228.6 \leq a < 304.8$	D
$304.8 \leq a < 381$	F
$a > 381$	CF

467 For the OCA ratings given in the above table, an example of the report OCA transition  
 468 matrix  $\mathbf{P}_{\text{Report}}$  is given as

$$469 \quad \mathbf{P}_{\text{Report}} = \begin{bmatrix} 7.76e-1 & 2.13e-1 & 5.25e-3 & 2.16e-3 & 1.85e-3 & 2.47e-3 \\ 0 & 9.28e-1 & 4.40e-2 & 1.74e-2 & 7.94e-3 & 2.60e-3 \\ 0 & 0 & 8.70e-1 & 1.19e-3 & 6.64e-3 & 4.78e-3 \\ 0 & 0 & 0 & 9.40e-1 & 5.03e-2 & 9.39e-3 \\ 0 & 0 & 0 & 0 & 8.65e-1 & 1.35e-1 \\ 0 & 0 & 0 & 0 & 0 & 1 \end{bmatrix}. \quad (32)$$

470 As discussed in Sec. 3, the reported OCA transition matrix may have errors due to the  
 471 human observation errors of the field engineers. Next, a demonstration is presented of how to  
 472 obtain the underlying true transition matrix based on the human error matrix using the proposed  
 473 method. After that, a discussion is presented on how to obtain a gap degradation model and  
 474 how to use it to perform diagnostics and prognostics.

475

#### 476 **4.1 Mapping the reported OCA transition matrix to the true OCA transition matrix for** 477 **different human error scenarios**

478 As indicated by [26], this human error/performance may be evaluated to quantify the  
 479 reliability or accuracy of these inspections. For demonstration purposes, four different cases as  
 480 shown in Eqs. (33) to (36) will be evaluated to see the effect of human error on the OCA  
 481 transition matrix and the degradation model. Case 1 assumes that the inspection is performed  
 482 without any human observation errors, in other words,  $\mathbf{P}_{\text{human}}$  would be the identity matrix.  
 483 Case 2 represents the behavior of an inspector that regularly tends to assess a structural  
 484 component to be in a better condition than reality. For example, as shown in Eq. (34), there is  
 485 a 4% probability that an inspector reports a rating A to a structural component when in reality  
 486 the true state of the component belongs to rating B. Contrarily, Case 3 represents an inspector

487 that tends to be very conservative. For example, as shown in Eq. (35), there is a 5% probability  
 488 that an inspector reports a rating F to a structural component when in reality the true state of  
 489 the component belongs to rating D. Case 4 represents a case in between Case 2 and Case 3.

490 
$$\mathbf{P}_{\text{human}}^{\text{case1}} = \mathbf{I}_{6 \times 6}, \quad (33)$$

491 
$$\mathbf{P}_{\text{human}}^{\text{case2}} = \begin{bmatrix} 1 & 0 & 0 & 0 & 0 & 0 \\ 0.04 & 0.96 & 0 & 0 & 0 & 0 \\ 0 & 0.40 & 0.60 & 0 & 0 & 0 \\ 0 & 0.03 & 0.17 & 0.80 & 0 & 0 \\ 0 & 0 & 0 & 0.03 & 0.97 & 0 \\ 0 & 0 & 0 & 0 & 0.03 & 0.97 \end{bmatrix}, \quad (34)$$

492 
$$\mathbf{P}_{\text{human}}^{\text{case3}} = \begin{bmatrix} 0.60 & 0.40 & 0 & 0 & 0 & 0 \\ 0 & 0.90 & 0.08 & 0.02 & 0 & 0 \\ 0 & 0 & 0.90 & 0.10 & 0 & 0 \\ 0 & 0 & 0 & 0.95 & 0.05 & 0 \\ 0 & 0 & 0 & 0 & 0.98 & 0.02 \\ 0 & 0 & 0 & 0 & 0 & 1 \end{bmatrix}, \quad (35)$$

493 
$$\mathbf{P}_{\text{human}}^{\text{case4}} = \begin{bmatrix} 0.9 & 0.1 & 0 & 0 & 0 & 0 \\ 0.05 & 0.9 & 0.03 & 0.02 & 0 & 0 \\ 0.04 & 0.06 & 0.8 & 0.05 & 0.035 & 0.015 \\ 0.015 & 0.035 & 0.05 & 0.8 & 0.6 & 0.04 \\ 0 & 0.015 & 0.035 & 0.05 & 0.8 & 0.1 \\ 0 & 0 & 0 & 0 & 0 & 1 \end{bmatrix}, \quad (36)$$

494 As shown in Eq. (10), the true OCA transition matrix ( $\mathbf{P}_{\text{OCA}}$ ) may be obtained after knowing  
 495 the reported OCA transition matrix ( $\mathbf{P}_{\text{Report}}$ , Eq. (32)) and the human observation error ( $\mathbf{P}_{\text{human}}$ ,  
 496 Eqs. (33) through (36)). Using the different cases for human observation errors mentioned  
 497 earlier, the true OCA transition matrix for each case is shown in Eqs. (37) to (40) respectively.

$$498 \quad \mathbf{P}_{OCA}^{case1} = \begin{bmatrix} 7.76e-1 & 2.13e-1 & 5.25e-3 & 2.16e-3 & 1.85e-3 & 2.47e-3 \\ 0 & 9.28e-1 & 4.40e-2 & 1.74e-2 & 7.94e-3 & 2.60e-3 \\ 0 & 0 & 8.70e-1 & 1.19e-3 & 6.64e-3 & 4.78e-3 \\ 0 & 0 & 0 & 9.40e-1 & 5.03e-2 & 9.39e-3 \\ 0 & 0 & 0 & 0 & 8.65e-1 & 1.35e-1 \\ 0 & 0 & 0 & 0 & 0 & 1 \end{bmatrix}, \quad (37)$$

$$499 \quad \mathbf{P}_{OCA}^{case2} = \begin{bmatrix} 7.02e-1 & 2.89e-1 & 7.01e-3 & 0 & 0 & 2.48e-3 \\ 0 & 9.08e-1 & 7.03e-2 & 1.06e-2 & 8.26e-3 & 2.49e-3 \\ 0 & 0 & 8.42e-1 & 1.47e-1 & 6.04e-3 & 4.73e-3 \\ 0 & 0 & 0 & 9.48e-1 & 4.55e-2 & 6.71e-3 \\ 0 & 0 & 0 & 0 & 8.60e-1 & 1.40e-1 \\ 0 & 0 & 0 & 0 & 0 & 1 \end{bmatrix}, \quad (38)$$

$$500 \quad \mathbf{P}_{OCA}^{case3} = \begin{bmatrix} 7.89e-1 & 2.02e-1 & 3.02e-3 & 1.42e-3 & 1.87e-3 & 2.35e-3 \\ 0 & 9.50e-1 & 2.72e-2 & 1.19e-2 & 8.10e-3 & 2.48e-3 \\ 0 & 0 & 8.40e-1 & 1.48e-1 & 4.27e-3 & 7.46e-3 \\ 0 & 0 & 0 & 8.66e-1 & 1.17e-1 & 1.74e-2 \\ 0 & 0 & 0 & 0 & 8.69e-1 & 1.31e-1 \\ 0 & 0 & 0 & 0 & 0 & 1 \end{bmatrix}, \quad (39)$$

501 and

$$502 \quad \mathbf{P}_{OCA}^{case4} = \begin{bmatrix} 5.63e-1 & 4.34e-1 & 3.17e-3 & 0 & 0 & 0 \\ 0 & 9.37e-1 & 4.11e-2 & 1.27e-2 & 7.80e-3 & 1.15e-3 \\ 0 & 0 & 8.93e-1 & 9.66e-2 & 8.35e-3 & 1.59e-3 \\ 0 & 0 & 0 & 9.29e-1 & 7.13e-2 & 0 \\ 0 & 0 & 0 & 0 & 9.14e-1 & 8.61e-2 \\ 0 & 0 & 0 & 0 & 0 & 1 \end{bmatrix}, \quad (40)$$

503 The human observation error has a significant effect on the true OCA transition matrix.

504 For Case 1, the true OCA transition matrix ( $\mathbf{P}_{OCA}^{case1}$ , Eq. (37)) is equal to the reported OCA  
505 transition matrix ( $\mathbf{P}_{Report}$ , Eq. (32)) and consistent when human observation error is not present.

506 For Case 2, the true OCA transition matrix ( $\mathbf{P}_{OCA}^{case2}$ , Eq. (38)) shows a decrease on the majority  
507 of the transition probabilities located in the diagonal when Cases 1 and 2 are compared. In  
508 other words, the degradation model should tend to deteriorate faster at the beginning.

509 Contrarily, the true OCA transition matrix ( $\mathbf{P}_{OCA}^{case3}$ , Eq. (39)) for Case 3 shows that the majority  
510 of the transition probabilities located in the diagonal shows an increase when Cases 1 and 3 are  
511 compared. Note that not all the diagonal elements show a decrease due to the *error*  
512 *cancellations* in first and second assessments of the OCA ratings. But in general, the  
513 degradation model of Case 3 degrades slower than that of Case 1 (as shown in the results in  
514 Sec. 4.2). As expected, Case 4 (i.e. Eq. (40)) shows some of the diagonal entries increase while  
515 the other diagonals entries decrease when Cases 1 and 4 are compared. Even though effects of  
516 the human observation errors on the transition matrix is very complicated due to the “error  
517 cancellation” in the OCA ratings, the proposed approach can account for the complicated  
518 effects by mapping the reported OCA transition matrix to the true OCA transition matrix.

519 In the next subsection, the underlying degradation models will be identified based on the  
520 obtained OCA transition matrices of different level of human observations errors.

521

## 522 4.2 Gap growth modeling based on OCA transition matrix

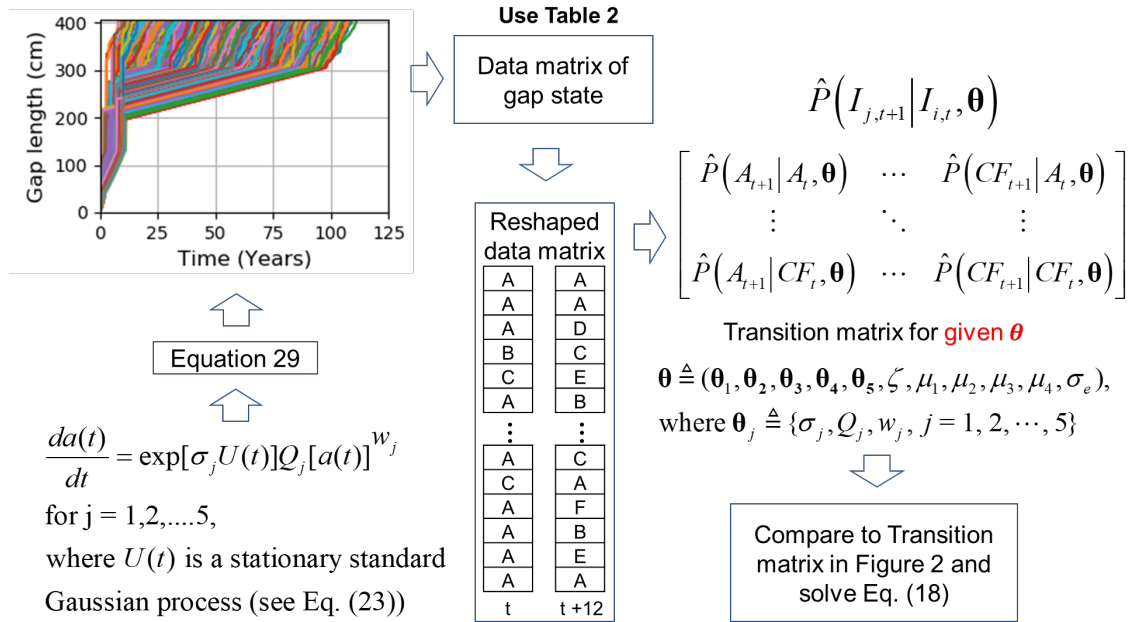
523 Figure 7 shows a flowchart of how to obtain the transition matrix from the stochastic  
524 degradation model, which is used to estimate the gap growth model parameters based on the  
525 OCA transition matrices obtained above.

526 Figure 8 shows the cumulative minimum error after each iteration of the stochastic  
527 degradation model after tuning 21 parameters for four different cases (i.e. Eq. (33) through  
528 (36)). The GSA optimization algorithm successfully achieves a very small error for each case.

529 Figure 9 presents the simulated gap growth curves corresponding to the four scenarios after  
530 identifying the optimal parameters of the gap growth model using GSA. Comparing the gap  
531 growth curves of Case 2 to 4 with Case 1, similar conclusions can be obtained as that from  
532 comparing the OCA transition matrices (i.e. Eq. (37)-(40)). For Case 2, the degradation model

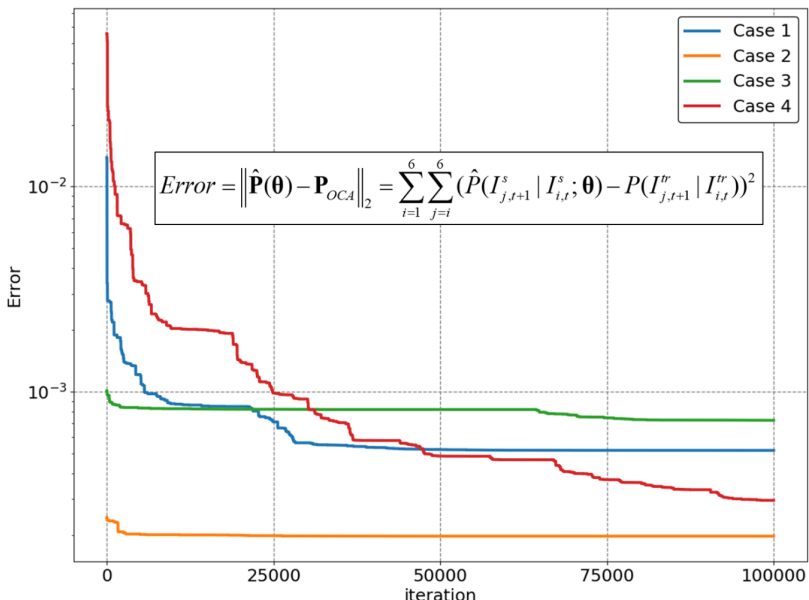


533 should tend to deteriorate faster at the beginning as shown in Fig. 9, which can also be seen in  
 534 Fig. 10 when comparing Case 1 and 2. Contrarily, for Case 3, the degradation model should  
 535 tend to deteriorate slower as shown in Fig. 9, when Cases 1 and 3 are compared.



536  
 537  
 538

**Figure 7:** Flowchart to obtain simulated transition matrix from a gap degradation model

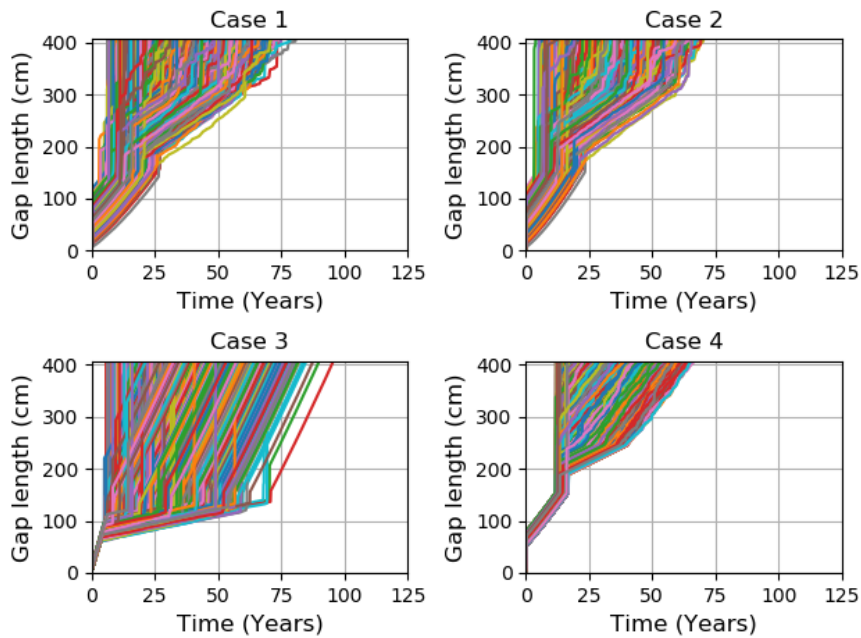


539  
 540

**Figure 8:** Cumulative minimum error after each iteration

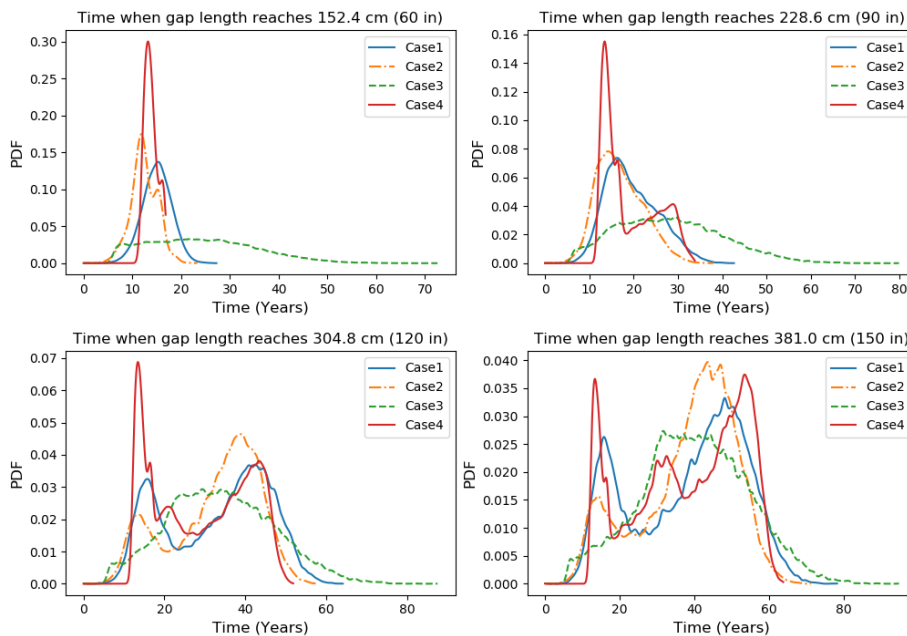
541 Fig. 10 shows the time distribution when the curves shown in Fig. 9 exceed four different  
 542 thresholds. As expected, the time distribution for Case 2 shifts to earlier time region (i.e. left)

543 compared to its counterpart of Case 1. Conversely, the time distribution for Case 3 shifts  
 544 towards later time region (i.e. right) if compared to Case 1. Consistently, the result for Case 4  
 545 in general shows time distributions between that of Case 2 and 3.



546  
 547

**Figure 9:** Gap growth model comparison for different human error cases



548  
 549  
 550

**Figure 10:** Time distribution when gap length,  $a$ , exceeds different damage thresholds for different human error cases

551 The above results show that the proposed method is able to effectively investigate the  
 552 effects of human errors on the OCA transition matrix and the gap growth of the gate over time.

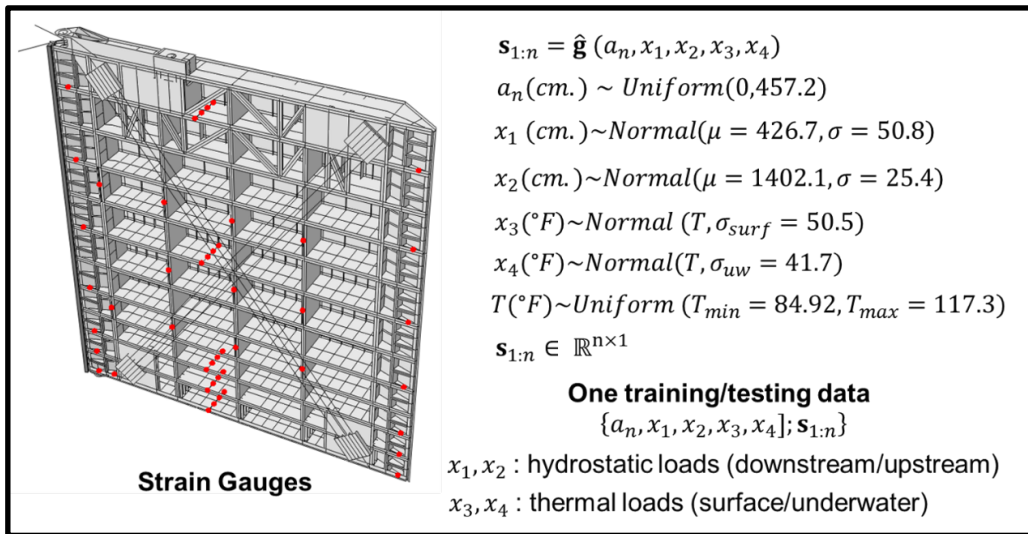
553

### 554 4.3 Bearing gap diagnosis and prognosis using SHM and gap growth modeling

555 Fig. 11 shows the locations where the strain gauges are installed based on the SHM strain  
556 network installed at the Greenup miter gate (Kentucky, USA). Data is extracted from a FE  
557 model of this gate to train a Kriging surrogate model.

558 Two different surrogate models are built, one that would be used to generate the synthetic  
559 data (representing the true physics) and the other to be calibrated during the estimation process.

560 In other words, one surrogate model is built to mimic the reality and the other one to mimic the  
561 FE model in the estimation process. Both surrogate models are built from the input and outputs  
562 of the FE model after space filling its parameter space. Figure 12(a) shows the updated  
563 predictions of the gap length against the true damage using the proposed gap growth model in  
564 the estimation process.

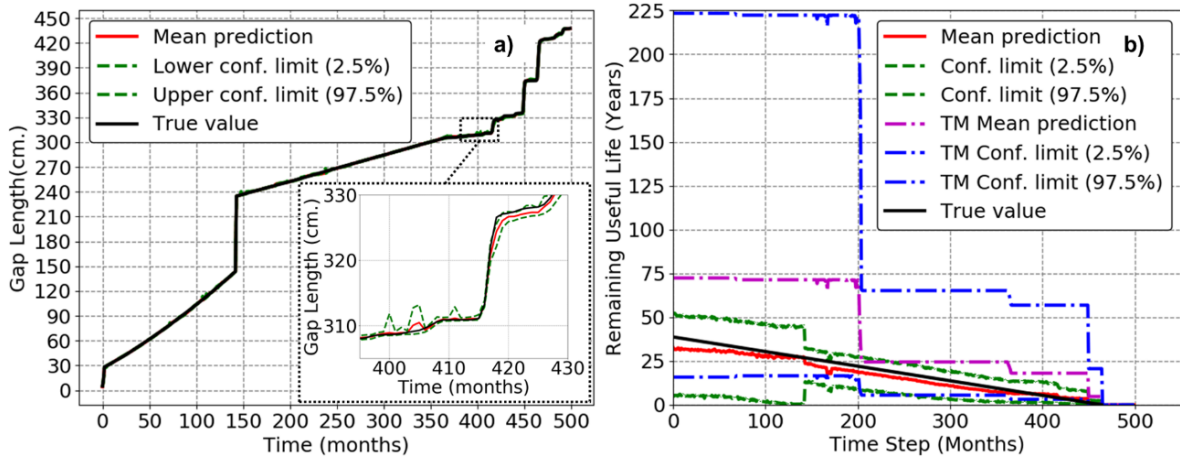


565  
566

**Figure 11:** Sensor locations, and data generated to train surrogate model

567 As shown in Figure 12(b), the proposed method can accurately capture remaining useful  
568 life (RUL) while effectively performing damage detection (i.e. Fig. 12 (a)). In addition, the  
569 results show that the uncertainty in the RUL estimate can be reduced significantly by mapping  
570 the OCA transition matrix into a higher-precision gap growth model, compared to that of the  
571 transition matrix-based method as reviewed in Sec. 3. The jumps in Figure 12(b) are attributed

572 to the discrete nature of the OCA ratings, which are more pronounced in the predictions using the  
 573 TM based approach. More details of the TM approach can be found in [16]. Results of this case  
 574 study demonstrate the efficacy of the proposed method.



575 **Figure 12:** (a) Damage detection over time, and (b) RUL using the proposed method (where  
 576 “TM” stands for the transition matrix-based approach as reviewed in [16])  
 577

578

579 **5 Discussion**

580 Failure prognostics plays a vital role in proactively scheduling maintenance activities to  
 581 avoid catastrophic failures, which improves reliability of civil infrastructure and reduce overall  
 582 life-cycle costs [34–37]. In recent years, data-driven approaches have been developed using  
 583 neural networks [24,38,39], deep learning [40], and other machine learning-based approaches  
 584 [41–44] to correlate sensor monitoring data with system degradation and in order to predict  
 585 system failures. For structures like miter gates, however, historical continuous monitoring data  
 586 is not available, which makes the state-of-the-art neural network-based approaches  
 587 inapplicable for failure prognostics of a miter gate. Instead, highly abstracted rating data are  
 588 available, which contain some kind of degradation information. Along with the highly  
 589 abstracted data, a high-fidelity physics-based finite element model has been developed to  
 590 provide some physical understanding of the gate strain response under different conditions. To  
 591 fully leverage the information of the abstracted ratings and the high-fidelity physics-based

592 simulation model, a new prognostic approach is required. To this end, this paper develops a  
593 novel hybrid failure prognostic approach by integrating the highly abstracted OCA ratings with  
594 structural health monitoring data.

595 The developed approach tackles the issue that no viable degradation model available exists  
596 for failure prognostics by mapping the corrected OCA transition matrix into a continuous-space  
597 degradation model using an optimization-based method. As an optimization-based approach,  
598 it is possible that there may be non-unique solutions. To address this issue, the authors plan to  
599 develop a fully Bayesian approach to quantify the uncertainty in various model parameters and  
600 continuously update the model parameters during the monitoring process methods such as  
601 dynamic Bayesian networks. Moreover, more constraints to the optimization model and the  
602 OCA transition matrix need to be added in the future to address the potential non-uniqueness  
603 issues in the estimation process.

604 In this paper, a Yang-Manning degradation model is assumed as a potential degradation  
605 model. Even though this flexible model allows capturing various gap-growth behavior classes  
606 without requiring detailed understanding of the underlying physics, it may not accurately  
607 represent the gap degradation pattern in reality. The assumed model may conflict with the  
608 subsequent measurement data obtained through an SHM procedure and then affect the  
609 inference of the damage states of the system. This is related to the potential model form  
610 uncertainty of the assumed degradation model. To address this challenge, the following two  
611 research topics are worth investigating in the future: (1) Bayesian model selection and updating  
612 using monitoring data to select the best degradation model from multiple candidate models and  
613 dynamically updating the model parameters; and (2) dynamic model uncertainty quantification  
614 to automatically correct the assumed degradation model during the monitoring process [45].

615 As mentioned earlier, the framework presented in this work can be applied to other  
616 structures with SHM systems installed where very little information about the deterioration

617 rate of a component or system exists, but abstracted inspection data based on ratings are  
618 available. For example, this methodology can be used for other structural components of miter  
619 gates with different failure modes (e.g., corrosion or pre-tension loss) or even other structures  
620 including bridges, pavements and offshore structures due to the availability of inspection  
621 ratings performed by several transportation and private agencies.

622

## 623 **6 Conclusions**

624 This paper presents a novel **hybrid** framework for failure diagnostics and prognostics for  
625 bearing damaged gaps in the quoin block components of a miter gate. **This framework is based**  
626 **on integrating abstracted inspection data and structural health monitoring data, with the**  
627 **following information as inputs:**

- 628 • **Historical visual inspection data given in rating/discrete form;**
- 629 • **Previous knowledge of the human observation errors (i.e.,  $P_{\text{human}}$ );**
- 630 • **A validated physics-based simulation model of the system;**
- 631 • **A known damage threshold to predict the failure;**
- 632 • **Structural health monitoring data (e.g., strain in the present case) at different locations.**

633 This work is especially useful when the evolution of the damage mechanism is not well  
634 known or understood either due to the lack of enough data that relates damage to sensor  
635 information or the lack of a physics-based model that describes the evolution of the damage. It  
636 is assumed that the only available data that describes the damage evolution are based on  
637 abstracted rating assessments such as the OCA ratings. An approach is first proposed to map  
638 the reported OCA transition matrix into the underlying true OCA transition matrix. Based on  
639 that, the proposed framework successfully integrates a stochastic degradation model built from

640 the OCA Markov transition matrix and shows how this model is suitable for integration with  
641 continuous monitoring.

642 The damage diagnosis via physics-based FE model updating using the degradation model  
643 proposed provides satisfactory results. Also, to demonstrate the improvement on the gap length  
644 prognosis, the updated over time RUL was compared against its true value. Results of a case  
645 study show that (1) the proposed framework can effectively address the issue of human  
646 reporting errors in the OCA ratings in the prognostics of miter gate, and (2) the uncertainty in  
647 the RUL estimate can be reduced significantly using the proposed framework.

648 Note that, this approach can be applicable to different components in miter gates, which may  
649 have different transition matrices values. However, further work needs to be done to extend this  
650 methodology from miter gate components to the miter gate system level (e.g. including all critical  
651 miter gate components); that work would need to focus on how failure mode probabilities from  
652 multiple causes/sources are correlated and propagate towards a more global limit state failure  
653 definition. In this paper, optimization-based methods are employed to identify the underlying  
654 true OCA transition matrices as well as the gap growth model parameters. These procedures  
655 can be integrated together in a full-Bayesian framework. The development of the full-Bayesian  
656 framework and the investigation of other alternative approaches will be studied in the future.

## 657 **Acknowledgements**

658 Funding for this work was provided by the US Army Corps of Engineers through the U.S.  
659 Army Engineer Research and Development Center Research Cooperative Agreement  
660 W912HZ-17-2-0024.

## 661 **Appendix A: Derivation of $\Pr\{I_t^{obs} = k, I_{t+1}^{obs} = q\}$**

662 The marginalization of  $\Pr\{I_{t+1}^{obs} = q, I_t^{obs} = k\} = \Pr\{I_{t+1}^{obs} = q | I_t^{obs} = k\} \Pr\{I_t^{obs} = k\}$  is shown  
663 as follows

$$\begin{aligned}
664 \quad \Pr\{I_{t+1}^{obs} = q, I_t^{obs} = k\} &= \sum_{i=1}^6 \sum_{j=i}^6 \Pr\{I_{t+1}^{obs} = q, I_t^{obs} = k, I_{t+1}^{tr} = j, I_t^{tr} = i\}, \\
&= \sum_{i=1}^6 \sum_{j=i}^6 \Pr\{(I_{t+1}^{obs} = q, I_t^{obs} = k) | (I_{t+1}^{tr} = j, I_t^{tr} = i)\} \Pr\{I_{t+1}^{tr} = j, I_t^{tr} = i\}.
\end{aligned} \tag{41}$$

665 According to the Bayesian network given in Fig. 5, it follows that

$$\begin{aligned}
666 \quad &\Pr\{(I_{t+1}^{obs} = q, I_t^{obs} = k) | (I_{t+1}^{tr} = j, I_t^{tr} = i)\} \\
&= \Pr\{I_{t+1}^{obs} = q | I_{t+1}^{tr} = j, I_t^{obs} = k\} \Pr\{I_t^{obs} = k | I_t^{tr} = i\}, \\
&= \frac{\Pr\{I_{t+1}^{obs} = q, I_{t+1}^{tr} = j, I_t^{obs} = k\}}{\sum_{w=k}^6 \Pr\{I_{t+1}^{obs} = w, I_{t+1}^{tr} = j, I_t^{obs} = k\}} P_{ik}^h.
\end{aligned} \tag{42}$$

667 Substituting Eq. (42) into Eq. (41) yields

$$\begin{aligned}
668 \quad &\Pr\{I_{t+1}^{obs} = q, I_t^{obs} = k\} \\
&= \sum_{i=1}^6 \sum_{j=i}^6 \left( \frac{\Pr\{I_{t+1}^{obs} = q, I_{t+1}^{tr} = j, I_t^{obs} = k\}}{\sum_{w=k}^6 \Pr\{I_{t+1}^{obs} = w, I_{t+1}^{tr} = j, I_t^{obs} = k\}} P_{ik}^h \right) \Pr\{I_{t+1}^{tr} = j, I_t^{tr} = i\}.
\end{aligned} \tag{43}$$

669 The following is obtained from the numerator of Eq. (6)

$$670 \quad \Pr\{I_{t+1}^{obs} = q, I_{t+1}^{tr} = j, I_t^{obs} = k\} = \Pr\{I_t^{obs} = k | I_{t+1}^{obs} = q, I_{t+1}^{tr} = j\} P_{jq}^h \Pr\{I_{t+1}^{tr} = j\}, \tag{44}$$

671 where  $\Pr\{I_{t+1}^{tr} = j\}$  is solved in Eq. (9). Then, combining Eqs. (43) and (44) yields

$$\begin{aligned}
672 \quad &P_{kq}^R \Pr\{I_t^{obs} = k\} \\
&= \sum_{i=1}^6 \sum_{j=i}^6 \left( \frac{\Pr\{I_t^{obs} = k | I_{t+1}^{obs} = q, I_{t+1}^{tr} = j\} P_{jq}^h \Pr\{I_{t+1}^{tr} = j\}}{\sum_{w=k}^6 \Pr\{I_t^{obs} = k | I_{t+1}^{obs} = w, I_{t+1}^{tr} = j\} P_{jw}^h \Pr\{I_{t+1}^{tr} = j\}} P_{ik}^h \right) \Pr\{I_{t+1}^{tr} = j, I_t^{tr} = i\}.
\end{aligned} \tag{45}$$

673

## 674 **Appendix B: A stochastic crack growth model by Yang and Manning [27]**

675 A simple second order approximation for a stochastic crack growth model was proposed

676 by Yang and Manning [27], given by



677 
$$\frac{da(t)}{dt} = X(t)Q(a(t))^w, \quad (46)$$

678 where  $Q$  and  $w$  are parameters that need to be estimated, and  $X(t)$  is modelled as a stationary  
 679 lognormal stochastic process with a unit mean and an auto-covariance function [27]

680 
$$\text{cov}(X(t_1), X(t_2)) = \sigma_x^2 \exp(-\zeta_x |t_2 - t_1|), \quad (47)$$

681 in which  $\sigma_x$  is the standard deviation of  $X(t)$ , and  $\zeta_x$  controls the correlation of  $X(t)$  over  
 682 time. If  $\zeta_x^{-1}$  approaches to zero,  $X(t)$  is a stationary lognormal white noise random process,  
 683 and the degradation model achieves its most non-conservative stochastic performance. On the  
 684 other hand, if  $\zeta_x^{-1}$  approaches infinity,  $X(t)$  is a lognormal random variable, and the model  
 685 becomes the most conservative.

686 In this paper, a model that is similar to the Yang and Manning model is selected since it  
 687 does not require a good understanding of the physics and maintains appropriate growth-law  
 688 features at the same time. The model is given by

689 
$$\frac{da(t)}{dt} = \exp(\sigma_i U(t))Q(a(t))^w, \quad (48)$$

690 in which  $\sigma_i > 0$  is a degradation stage-dependent variable and  $U(t)$  is a stationary standard  
 691 Gaussian process with auto-correlation function given by

692 
$$\text{cov}(U(t_1), U(t_2)) = \exp(-\zeta |t_2 - t_1|), \quad (49)$$

693 where  $\zeta$  is a correlation related parameter similar to Eq. (47). In addition, it is assumed that  
 694 the degradation model  $a_i = g(t, \theta)$  consists of  $N_d$  distinct degradation stages ( $N_d = 5$  in the  
 695 studied case). Thus, the multi-stage gap growth model is defined as

696 
$$\frac{da(t)}{dt} = \exp(\sigma_i U(t))Q_i(a(t))^w, i = 1, 2, \dots, N_d, \quad (50)$$

697 where  $a(t)$  is the gap length at time  $t$ ,  $\sigma_i$  is a standard deviation variable of degradation stage  
698  $i$ , and  $Q_i$  and  $w_i$  are degradation stage-dependent constants.

699

### 700 **Appendix C: Estimation of $\hat{P}(I_{j,t+1}^s | I_{i,t}^s; \theta, \mathbf{e})$ based on the simulation of gap growth**

701 As mentioned previously,  $\hat{\mathbf{P}}(\theta) \triangleq \{\hat{P}(I_{j,t+1}^s | I_{i,t}^s; \theta), i = 1, 2, \dots, 6; j = i, \dots, 6\}$ , for a given

702  $\mathbf{e} \triangleq \{e_1, e_2, \dots, e_{N_d-1}\}$ ,  $\hat{P}(I_{j,t+1}^s | I_{i,t}^s; \theta, \mathbf{e})$  is given by

$$703 \quad \hat{P}(I_{j,t+1}^s | I_{i,t}^s; \theta, \mathbf{e}) = \frac{P(I_{j,t+1}^s \cap I_{i,t}^s; \theta, \mathbf{e})}{P(I_{i,t}^s; \theta, \mathbf{e})}, \quad (51)$$

704 where

$$705 \quad P(I_{i,t}^s; \theta, \mathbf{e}) = \begin{cases} \Pr\{0 \leq a(t) < \beta_i\}, & \text{if } i = 1, \\ \Pr\{\beta_{i-1} \leq a(t) < \beta_i\}, & \text{if } 1 < i < 6, \forall i = 1, 2, \dots, 6 \\ \Pr\{\beta_{i-1} \leq a(t) < \infty\}, & \text{if } i = 6, \end{cases} \quad (52)$$

$$706 \quad P(I_{j,t+1}^s \cap I_{i,t}^s; \theta, \mathbf{e}) = \Pr\{\beta_{i-1} \leq a(t) < \beta_i \cap \beta_{j-1} \leq a(t+12) < \beta_j\}, \quad (53)$$

$\forall i = 1, 2, \dots, 6; j = i, \dots, 6,$

707 in which  $\beta_0 = 0$ ,  $a(t)$ , and  $a(t+12)$  are obtained through the degradation model given in Sec.  
708 3.3.1, conditioned on given  $\theta$  and  $\mathbf{e}$ , and  $\beta_i = \infty$  or  $\beta_j = \infty$  if  $i=6$  or  $j=6$ . The two time steps  
709 used in Eq. (53) are  $t$  and  $t+12$  since the inspection interval in the forthcoming case study is  
710 one year, and the unit of the time step of the discrete time degradation model (i.e., Eqs. (24)  
711 and (25)) is one month.

712 Since the inspection time  $t$  can be any time in the lifetime of the gate, Eqs. (51) through  
713 (53) are rewritten as follows

$$\begin{aligned}
& \hat{P}(I_{j,t+1}^s | I_{i,t}^s; \boldsymbol{\theta}, \mathbf{e}) \\
714 \quad & = \int_{t_l}^{t_u} \hat{P}(I_{j,t+1}^s | I_{i,t}^s; \boldsymbol{\theta}, \mathbf{e}, t) f(t) dt, \quad (54) \\
& = \int_{t_l}^{t_u} \frac{\Pr\{\beta_{i-1} \leq a(t) < \beta_i \cap \beta_{j-1} \leq a(t+12) < \beta_j\}}{\Pr\{\beta_{i-1} \leq a(t) < \beta_i\}} \frac{1}{t_u - t_l} dt,
\end{aligned}$$

715 where  $f(t)$  represents the distribution of the time duration of interest. This distribution is  
716 assumed as a uniform distribution bounded by  $t_l$  and  $t_u$ , which are respectively the lower and  
717 upper bounds of the time duration of interest.

718 In general, Eqs. (54) is analytically intractable due to the complicated transition between  
719 stages, even though several analytical expressions have been developed for the degradation  
720 model with only one stage based on assumptions and simplifications [27]. In this paper, a  
721 simulation-based method is employed. For a given  $\boldsymbol{\theta}$  and  $\mathbf{e}$ , the degradation of the gap is first  
722 simulated using the discrete-time model given in Eqs. (24) and (25). From the simulation, the  
723 samples obtained of the gap length are denoted as  
724  $\mathbf{a}_s(\boldsymbol{\theta}, \mathbf{e}) \triangleq \{a_{i,j}, i = 1, 2, \dots, n_{MCS}; j = 1, 2, \dots, N_t\}$ , where  $a_{i,j}$  is the  $i$ -th realization of the gap  
725 growth curve at time step  $t_j$ ,  $n_{MCS}$  is the number of samples at each time step, and  $N_t$  is the  
726 total number of simulation time steps. Based on the simulated samples of the gap growth, Eq.  
727 (54) is approximated as

$$728 \quad \hat{P}(I_{j,t+1}^s | I_{i,t}^s; \boldsymbol{\theta}, \mathbf{e}) \approx \frac{1}{N_t - 12} \sum_{k=1}^{N_t-12} \frac{\Pr\{\beta_{i-1} \leq a(t_k) < \beta_i \cap \beta_{j-1} \leq a(t_k + 12) < \beta_j\}}{\Pr\{\beta_{i-1} \leq a(t_k) < \beta_i\}}. \quad (55)$$

729 In the above equation,  $\frac{\Pr\{\beta_{i-1} \leq a(t_k) < \beta_i \cap \beta_{j-1} \leq a(t_k + 12) < \beta_j\}}{\Pr\{\beta_{i-1} \leq a(t_k) < \beta_i\}}$  is estimated using  $\mathbf{a}_s$  as

$$\begin{aligned}
& \frac{\Pr\{\beta_{i-1} \leq a(t_k) < \beta_i \cap \beta_{j-1} \leq a(t_k + 12) < \beta_j\}}{\Pr\{\beta_{i-1} \leq a(t_k) < \beta_i\}} \\
730 \quad & \approx \frac{1}{n_{MCS}} \frac{\sum_{q=1}^{n_{MCS}} \Lambda((\beta_{i-1} \leq a_{q,k} < \beta_i) \cap (\beta_{j-1} \leq a_{q,k+12} < \beta_j))}{\sum_{q=1}^{n_{MCS}} \Lambda(\beta_{i-1} \leq a_{q,k} < \beta_i)}, \quad (56)
\end{aligned}$$

731 where  $\Lambda(E)$  is an indicator function such  $\Lambda(E) = 1$  if event  $E$  is true and  $\Lambda(E) = 0$  if event

732  $E$  is false. In the above equation, event  $E$  represents  $(\beta_{i-1} \leq a_{q,k} < \beta_i) \cap (\beta_{j-1} \leq a_{q,k+12} < \beta_j)$

733 and  $\beta_i \leq a_{q,k} < \beta_{i+1}$ .

### 734 References

- 735 [1] U.S. Army Corps of Engineers Headquarters. Navigation 2018.  
736 <http://www.usace.army.mil/Missions/CivilWorks/Navigation.aspx> (accessed August 1, 2018).
- 737 [2] Eick BA, Treece ZR, Spencer BF, Smith MD, Sweeney SC, Alexander QG, et al. Automated  
738 damage detection in miter gates of navigation locks. *Struct Control Heal Monit* 2018;25:1–18.  
739 <https://doi.org/10.1002/stc.2053>.
- 740 [3] Foltz SD. Investigation of Mechanical Breakdowns Leading to Lock Closures. Champaign, IL:  
741 2017.
- 742 [4] Przybyla J. Best Practices in Asset Management. Alexandria, Virginia: 2013.
- 743 [5] USACE. Policy for Operational Condition Assessments of USACE Assets 2019:13.  
744 <https://www.publications.usace.army.mil/Portals/76/Users/182/86/2486/EC-11-2-218.pdf?ver=2019-09-04-162858-440>.
- 746 [6] U.S. Army Corps of Engineers Headquarters. SMART GATE 2007.  
747 <https://www.erdc.usace.army.mil/Media/Fact-Sheets/Fact-Sheet-Article-View/Article/476668/smart-gate/> (accessed August 1, 2018).
- 749 [7] Graybeal BA, Phares BM, Rolander DD, Moore M, Washer G. Visual inspection of highway  
750 bridges. *J Nondestruct Eval* 2002;21:67–83. <https://doi.org/10.1023/A:1022508121821>.
- 751 [8] Orcesi AD, Cremona CF. A bridge network maintenance framework for Pareto optimization of  
752 stakeholders/users costs. *Reliab Eng Syst Saf* 2010;95:1230–43.  
753 <https://doi.org/10.1016/j.res.2010.06.013>.
- 754 [9] Calvert G, Neves L, Andrews J, Hamer M. Multi-defect modelling of bridge deterioration using  
755 truncated inspection records. *Reliab Eng Syst Saf* 2020;200.  
756 <https://doi.org/10.1016/j.res.2020.106962>.
- 757 [10] Zhang X, Gao H. Road maintenance optimization through a discrete-time semi-Markov decision  
758 process. *Reliab Eng Syst Saf* 2012;103:110–9. <https://doi.org/10.1016/j.res.2012.03.011>.
- 759 [11] Abaza KA. Empirical approach for estimating the pavement transition probabilities used in non-  
760 homogenous Markov chains. *Int J Pavement Eng* 2017;18:128–37.  
761 <https://doi.org/10.1080/10298436.2015.1039006>.
- 762 [12] Zhang Y, Kim C-W, Tee KF. Maintenance management of offshore structures using Markov  
763 process model with random transition probabilities. *Struct Infrastruct Eng* 2017;13:1068–80.  
764 <https://doi.org/10.1080/15732479.2016.1236393>.
- 765 [13] Mohseni H, Setunge S, Zhang G, Wakefield R. Markov Process for Deterioration Modeling and

- 766 Asset Management of Community Buildings. *J Constr Eng Manag* 2017;143:04017003.  
767 [https://doi.org/10.1061/\(ASCE\)CO.1943-7862.0001272](https://doi.org/10.1061/(ASCE)CO.1943-7862.0001272).
- 768 [14] Niu G, Yang B-S, Pecht M. Development of an optimized condition-based maintenance system  
769 by data fusion and reliability-centered maintenance. *Reliab Eng Syst Saf* 2010;95:786–96.  
770 <https://doi.org/10.1016/j.res.2010.02.016>.
- 771 [15] Wang C, Elsayed EA. Stochastic modeling of corrosion growth. *Reliab Eng Syst Saf*  
772 2020;204:107120. <https://doi.org/10.1016/j.res.2020.107120>.
- 773 [16] Vega MA, Hu Z, Todd MD. Optimal maintenance decisions for deteriorating quoin blocks in  
774 miter gates subject to uncertainty in the condition rating protocol. *Reliab Eng Syst Saf* 2020;204.  
775 <https://doi.org/10.1016/j.res.2020.107147>.
- 776 [17] Alaswad S, Xiang Y. A review on condition-based maintenance optimization models for  
777 stochastically deteriorating system. *Reliab Eng Syst Saf* 2017;157:54–63.  
778 <https://doi.org/10.1016/j.res.2016.08.009>.
- 779 [18] Baraldi P, Mangili F, Zio E. Investigation of uncertainty treatment capability of model-based  
780 and data-driven prognostic methods using simulated data. *Reliab Eng Syst Saf* 2013;112:94–  
781 108. <https://doi.org/10.1016/j.res.2012.12.004>.
- 782 [19] Vega MA, Ramancha MR, Conte JP, Todd MD. Efficient Bayesian Inference of Miter Gates  
783 using High-Fidelity Models. 38th Int. Modal Anal. Conf., Houston, Texas: Springer; 2021.
- 784 [20] Ramancha MK, Astroza R, Conte JP, Restrepo JI, Todd MD. Bayesian Nonlinear Finite Element  
785 Model Updating of a Full-Scale Bridge-Column using Sequential Monte Carlo. 38th Int. Modal  
786 Anal. Conf., Houston, Texas: Springer; 2020.
- 787 [21] Yang Y, Madarshahian R, Todd MD. Bayesian Damage Identification Using Strain Data from  
788 Lock Gates, Springer,; 2019, p. 47–54. [https://doi.org/10.1007/978-3-030-12115-0\\_7](https://doi.org/10.1007/978-3-030-12115-0_7).
- 789 [22] Gomez F, Spencer, Jr. BF, Smith MD. Bayesian Modeling Updating of Miter Gates with  
790 Uncertain Boundary Conditions. *Struct. Heal. Monit.* 2019, Lancaster, PA: DEStech  
791 Publications, Inc.; 2019. <https://doi.org/10.12783/shm2019/32129>.
- 792 [23] Smith M, Fillmore T. Methodology supporting Civil Works implementation of tainter gate  
793 trunnion friction structural health monitoring. 2018. <https://doi.org/10.21079/11681/29975>.
- 794 [24] Vega MA, Todd MD. A variational Bayesian neural network for structural health monitoring  
795 and cost-informed decision-making in miter gates. *Struct Heal Monit* 2020.  
796 <https://doi.org/10.1177/1475921720904543>.
- 797 [25] Vega MA, Madarshahian R, Fillmore TB, Todd MD. Optimal Maintenance Decision for  
798 Deteriorating Components in Miter Gates Using Markov Chain Prediction Model. *Struct. Heal.*  
799 *Monit.* 2019 Enabling Intell. Life-cycle Heal. Manag. Ind. Internet Things, Lancaster, PA:  
800 DEStech Publications, Inc.; 2019, p. 1471–8. <https://doi.org/10.12783/shm2019/32269>.
- 801 [26] Campbell LE, Connor RJ, Whitehead JM, Washer GA. Benchmark for Evaluating Performance  
802 in Visual Inspection of Fatigue Cracking in Steel Bridges. *J Bridg Eng* 2020;25:04019128.  
803 [https://doi.org/10.1061/\(ASCE\)BE.1943-5592.0001507](https://doi.org/10.1061/(ASCE)BE.1943-5592.0001507).
- 804 [27] Yang JN, Manning SD. A simple second order approximation for stochastic crack growth  
805 analysis. *Eng Fract Mech* 1996;53:677–86. [https://doi.org/10.1016/0013-7944\(95\)00130-1](https://doi.org/10.1016/0013-7944(95)00130-1).
- 806 [28] Xiang Y, Gubian S, Suomela B, Hoeng J. Generalized Simulated Annealing for Global  
807 Optimization: The GenSA Package. *R J* 2013;5:13. <https://doi.org/10.32614/RJ-2013-002>.
- 808 [29] Xiang Y, Gong XG. Efficiency of generalized simulated annealing. *Phys Rev E* 2000;62:4473–  
809 6. <https://doi.org/10.1103/PhysRevE.62.4473>.
- 810 [30] Hoskere V, Eick B, Spencer BF, Smith MD, Foltz SD. Deep Bayesian neural networks for  
811 damage quantification in miter gates of navigation locks. *Struct Heal Monit*  
812 2019;147592171988208. <https://doi.org/10.1177/1475921719882086>.
- 813 [31] Eick BA, Treece, Zachary R., Spencer Jr. BF, Smith MD, Sweeney SC, Alexander QG, Foltz  
814 SD. Miter Gate Gap Detection Using Principal Component Analysis. 2017.

- 815 [32] Vega M, Madarshahian R, Todd MD. A Neural Network Surrogate Model for Structural Health  
816 Monitoring of Miter Gates in Navigation Locks. 37th Int. Modal Anal. Conf., Orlando, Florida:  
817 2019, p. 93–8. [https://doi.org/10.1007/978-3-030-12075-7\\_9](https://doi.org/10.1007/978-3-030-12075-7_9).
- 818 [33] Daniel R, Paulus T. Hydraulic Gates in View of Asset Management. Lock Gates Other Closures  
819 Hydraul. Proj., Elsevier; 2019, p. 945–60. <https://doi.org/10.1016/B978-0-12-809264-4.00017-3>.  
820 3.
- 821 [34] Zhao Y. On preventive maintenance policy of a critical reliability level for system subject to  
822 degradation. Reliab Eng Syst Saf 2003;79:301–8. [https://doi.org/10.1016/S0951-8320\(02\)00201-6](https://doi.org/10.1016/S0951-8320(02)00201-6).  
823 8320(02)00201-6.
- 824 [35] van Noortwijk JM, Frangopol DM. Deterioration and Maintenance Models for Insuring Safety  
825 of Civil Infrastructures at Lowest Life-Cycle Cost. Life-Cycle Perform. Deterior. Struct.,  
826 Reston, VA: American Society of Civil Engineers; 2003, p. 384–91.  
827 [https://doi.org/10.1061/40707\(240\)39](https://doi.org/10.1061/40707(240)39).
- 828 [36] Le Son K, Fouladirad M, Barros A, Levrat E, Iung B. Remaining useful life estimation based on  
829 stochastic deterioration models: A comparative study. Reliab Eng Syst Saf 2013;112:165–75.  
830 <https://doi.org/10.1016/j.ress.2012.11.022>.
- 831 [37] Li R, Arzaghi E, Abbassi R, Chen D, Li C, Li H, et al. Dynamic maintenance planning of a  
832 hydro-turbine in operational life cycle. Reliab Eng Syst Saf 2020;204:107129.  
833 <https://doi.org/10.1016/j.ress.2020.107129>.
- 834 [38] Zhang X, Xiao L, Kang J. Degradation Prediction Model Based on a Neural Network with  
835 Dynamic Windows. Sensors 2015;15:6996–7015. <https://doi.org/10.3390/s150306996>.
- 836 [39] Khan F, Eker O, Khan A, Orfali W. Adaptive Degradation Prognostic Reasoning by Particle  
837 Filter with a Neural Network Degradation Model for Turbofan Jet Engine. Data 2018;3:49.  
838 <https://doi.org/10.3390/data3040049>.
- 839 [40] Zhang L, Gao H, Wen J, Li S, Liu Q. A deep learning-based recognition method for degradation  
840 monitoring of ball screw with multi-sensor data fusion. Microelectron Reliab 2017;75:215–22.  
841 <https://doi.org/10.1016/j.microrel.2017.03.038>.
- 842 [41] Zio E, Di Maio F. A data-driven fuzzy approach for predicting the remaining useful life in  
843 dynamic failure scenarios of a nuclear system. Reliab Eng Syst Saf 2010;95:49–57.  
844 <https://doi.org/10.1016/j.ress.2009.08.001>.
- 845 [42] Mohanty S, Das S, Chattopadhyay A, Peralta P. Gaussian Process Time Series Model for Life  
846 Prognosis of Metallic Structures. J Intell Mater Syst Struct 2009;20:887–96.  
847 <https://doi.org/10.1177/1045389X08099602>.
- 848 [43] Galar D, Kumar U, Lee J, Zhao W. Remaining Useful Life Estimation using Time Trajectory  
849 Tracking and Support Vector Machines. J Phys Conf Ser 2012;364:012063.  
850 <https://doi.org/10.1088/1742-6596/364/1/012063>.
- 851 [44] Ye Z-S, Xie M. Stochastic modelling and analysis of degradation for highly reliable products.  
852 Appl Stoch Model Bus Ind 2015;31:16–32. <https://doi.org/10.1002/asmb.2063>.
- 853 [45] Hu Z, Hu C, Mourelatos ZP, Mahadevan S. Model Discrepancy Quantification in Simulation-  
854 Based Design of Dynamical Systems. J Mech Des 2019;141:1–13.  
855 <https://doi.org/10.1115/1.4041483>.
- 856